



**HAL**  
open science

## **Tripling of western US particulate pollution from wildfires in a warming climate**

Yuanyu Xie, Meiyun Lin, Bertrand Decharme, Christine Delire, Larry Horowitz, David Lawrence, Fang Li, Roland Séférian

► **To cite this version:**

Yuanyu Xie, Meiyun Lin, Bertrand Decharme, Christine Delire, Larry Horowitz, et al.. Tripling of western US particulate pollution from wildfires in a warming climate. Proceedings of the National Academy of Sciences of the United States of America, 2022, 119 (14), 10.1073/pnas.2111372119 . hal-03624043

**HAL Id: hal-03624043**

**<https://hal.science/hal-03624043>**

Submitted on 30 Mar 2022

**HAL** is a multi-disciplinary open access archive for the deposit and dissemination of scientific research documents, whether they are published or not. The documents may come from teaching and research institutions in France or abroad, or from public or private research centers.

L'archive ouverte pluridisciplinaire **HAL**, est destinée au dépôt et à la diffusion de documents scientifiques de niveau recherche, publiés ou non, émanant des établissements d'enseignement et de recherche français ou étrangers, des laboratoires publics ou privés.

1 Tripling of Western US Particulate Pollution from Wildfires in a Warming  
2 Climate

3

4 Yuanyu Xie<sup>1,2\*</sup>, Meiyun Lin<sup>1,2\*</sup>, Bertrand Decharme<sup>3</sup>, Christine Delire<sup>3</sup>, Larry W. Horowitz<sup>2</sup>, David M.  
5 Lawrence<sup>4</sup>, Fang Li<sup>5</sup>, Roland Séférian<sup>3</sup>

6 <sup>1</sup>Atmospheric and Oceanic Sciences, Princeton University, Princeton, NJ, USA,

7 <sup>2</sup>NOAA Geophysical Fluid Dynamics Laboratory, Princeton, NJ, USA

8 <sup>3</sup>CNRM, Université de Toulouse, Météo - France, CNRS, Toulouse, France,

9 <sup>4</sup>Climate and Global Dynamics Laboratory, National Center for Atmospheric Research,  
10 Boulder, CO, USA

11 <sup>5</sup>International Center for Climate and Environment Sciences, Institute of Atmospheric Physics, Chinese  
12 Academy of Sciences, Beijing, China

13

14 **\*Corresponding authors:** Yuanyu Xie (Email: [Yuanyu.Xie@noaa.gov](mailto:Yuanyu.Xie@noaa.gov); Phone:609-865-0982)

15 Meiyun Lin (Email: [Meiyun.Lin@noaa.gov](mailto:Meiyun.Lin@noaa.gov); Phone: 609-937-9129)

16

17 **Author Contributions:** MYL conceived this study and designed the research. YYX and MYL performed  
18 the analyses and wrote the article. All coauthors contributed to discussions and improving the manuscript.

19 **Competing Interest Statement:** The authors declare no competing interests.

20 **Classification:** Physical Sciences (Earth, Atmospheric, and Planetary Sciences)

21 **Keywords:** Air quality, fires, drought, climate warming, Earth system models

22 **Submitted to PNAS on June 22, 2021; revised on November 19, 2021 and January 26, 2022**

23 **This PDF file includes:**

24 Main Text (~7785 words)

25 Figures 1 to 7

26

**Abstract (250 words)**

The air quality impact of increased wildfires in a warming climate has often been overlooked in current model projections, owing to the lack of interactive fire emissions of gases and particles responding to climate change in Earth System Model (ESM) projection simulations. Here we combine multi-ensemble projections of wildfires in three ESMs from the Sixth Coupled Model Intercomparison Project (CMIP6) with an empirical statistical model to predict fine particulate ( $PM_{2.5}$ ) pollution in the late 21<sup>st</sup> century under a suite of Shared Socioeconomic Pathways (SSPs). Total  $CO_2$  emissions from fires over western North America during August–September are projected to increase from present-day values by 60–110% (model spread) under a strong-mitigation scenario (SSP1-2.6), 100–150% under a moderate-mitigation scenario (SSP2-4.5), and 130–260% under a low-mitigation scenario (SSP5-8.5) in 2080–2100. We find that enhanced wildfire activity under SSP2-4.5 and SSP5-8.5 could cause a two- to three-fold increase in  $PM_{2.5}$  pollution over the US Pacific Northwest during August–September. Even with strong mitigation under SSP1-2.6,  $PM_{2.5}$  in the western US would increase ~50% by mid-century. By 2080–2100 under SSP5-8.5, the 95<sup>th</sup> percentile of late summer daily  $PM_{2.5}$  may frequently reach unhealthy levels of 55–150  $\mu g/m^3$ . In contrast, chemistry-climate models using prescribed fire emissions of particles not responding to climate change simulate only a 7% increase in  $PM_{2.5}$ . The consequential pollution events caused by large fires during 2017–2020 might become a new norm by the late 21<sup>st</sup> century, with a return period of every 3 to 5 years under SSP5-8.5 and SSP2-4.5.

**Significance Statement (120 words)**

Record-setting fires in the western US over the last decade caused severe air pollution, loss of human life, and property damage. Enhanced drought and increased biomass in a warmer climate may fuel larger and more frequent wildfires in the coming decades. Applying an empirical statistical model to fires projected by Earth system models including climate-ecosystem-socioeconomic interactions, we show that fine particulate pollution over the US Pacific Northwest could double to triple during late summer to fall by the end of the 21<sup>st</sup> century under intermediate- and low-mitigation scenarios. The historic fires and resulting pollution extremes of 2017–2020 could occur every 3 to 5 years under 21<sup>st</sup>

century climate change, posing challenges for regional air quality management and threatening public health.

## **Main Text**

### **Introduction**

Wildfires contribute 15–30% of atmospheric primary fine particle (PM<sub>2.5</sub>) emissions in the United States (1), with implications for ecosystems, human health, and climate (2-5). Marked increases in wildfire burned area over the western US in recent decades have been linked to anthropogenic climate change and land management practices (4, 6-8). Increasing emissions from wildfires have caused summertime PM<sub>2.5</sub> levels to rise in some western US regions despite efforts to control anthropogenic emissions (9-11). Millions of people were exposed to very unhealthy or hazardous PM<sub>2.5</sub> concentrations (150–650 µg/m<sup>3</sup> for 24-h average) for extended periods during recent large wildfires around the world (11-17). Exposure to dense smoke from fires has detrimental effects on human health (3, 18-20), with an economic cost due to short-term smoke exposure estimated to be \$11–20 billion per year in the continental US (21). The US Clean Air Act allows for screening of air quality exceedances caused by “exceptional events,” such as wildfires, from counting towards a non-attainment determination (22). Understanding the extent to which wildfire emissions in a future climate influence PM<sub>2.5</sub> exceedances thus has implications for designing effective air quality policies.

A number of studies have projected enhanced wildfire activity over the western US under a warming climate during the 21<sup>st</sup> century (23-27). However, owing to the lack of interactive fire emissions of gases and particles responding to climate change in current chemistry-climate models, projections of future PM<sub>2.5</sub> air quality generally overlook the impacts of changing fires (28-31). A few studies estimated future fire emissions using statistical regressions of burned area and climate variables and fed these emissions into an offline chemical transport model to estimate future PM<sub>2.5</sub> air quality (26, 32-35). These studies suggested 80–170% increases in fire emissions of primary aerosols by the 2050s, which resulted in 46–70% increases in surface organic carbon concentrations (a key component in fire smoke). Using fire emissions simulated by a process-based fire model driven by archived meteorological fields from a chemistry-climate model, several studies estimated 50–90% increases in mean organic carbon concentrations over the continental US by the late 21<sup>st</sup> century (23,

36). These results have large uncertainties, as the statistical or offline fire models typically do not include feedbacks among climate, land use, ecosystem dynamics, and anthropogenic influences through ignition and suppression (2, 37-39).

Here we leverage the Sixth Coupled Model Intercomparison Project (CMIP6) multi-model and multi-ensemble simulations of fire CO<sub>2</sub> emissions responding to changes in climate, vegetation, and population distributions, combined with a multiple linear regression (MLR) model developed from historical observations, to project wildfire impacts on PM<sub>2.5</sub> means and extremes over the western US under a suite of Shared Socioeconomic Pathways (SSPs; see *Methods*). The process-based fire models in CMIP6 are greatly improved compared to those in CMIP5, with better representation of the impacts of fuel wetness on fire occurrence and spread, enhanced fire spread rate in forest crowns, and ability to simulate multi-day fires (40-51). Our statistical model considers the influence of both local and regional fires, as well as inter-state smoke transport, air stagnation, and other meteorological conditions. We compare our MLR-predicted PM<sub>2.5</sub> with that simulated in the chemistry-climate models using prescribed fire emissions of gases and particles not responding to climate change (see *Methods*) (29). We show that drought and increased biomass under a warmer climate in the Pacific Northwest during the late 21<sup>st</sup> century increase the risk of fires, causing a two- to three-fold increase in PM<sub>2.5</sub> levels in late summer to fall.

## Results

### Observed correlations between fires and PM<sub>2.5</sub> air quality

[\[Figure 1 about here\]](#)

We first use historical observations to investigate the extent to which the interannual variability of PM<sub>2.5</sub> means and extremes at US surface sites can be explained by regional versus local fires as well as meteorological conditions. The observed relationships will serve as a basis for developing the MLR model used to predict future PM<sub>2.5</sub> levels from fire CO<sub>2</sub> emissions and meteorology available from CMIP6 Earth system models. We correlate surface PM<sub>2.5</sub> observations averaged over a 2°×2° grid with fire CO<sub>2</sub> emissions integrated over a box with size varying from 2.5°×2.5° to 20°×20° centered at that grid during May–November from 1997 to 2020, using simple linear regression and multiple linear

regression (MLR, see *Methods*). We consider four meteorological variables: surface temperature, precipitation, relative humidity, and air stagnation, which have been previously shown to be correlated with surface PM<sub>2.5</sub> (11, 52).

During August and September, when fires peak seasonally over the Pacific Northwest under the present-day climate (53), mean PM<sub>2.5</sub> levels at western US sites show strong correlations ( $r^2 = 0.5\text{--}0.9$ ) with regional fire CO<sub>2</sub> emissions summed over a box of 10°×10° to 15°×15°, indicating the importance of regional smoke transport (11) (Fig.1a). In comparison, the correlations are much weaker ( $r^2 < 0.5$ ) during May–July and October–November (Fig.S1), and are statistically insignificant ( $p > 0.05$ ) at most eastern US sites, where fire is not the dominant source of surface PM<sub>2.5</sub>. In the following analyses we thus focus on the US Pacific Northwest (solid black box on Fig.1b) during August and September.

The MLR model, including the impacts from meteorological variables, achieves higher correlations ( $r^2 = 0.7\text{--}0.9$ ; Fig.1b) compared to a simple linear regression with fires alone ( $r^2 = 0.5\text{--}0.9$ ; Fig.1a). Fire CO<sub>2</sub> emissions on average explain 66% of the observed PM<sub>2.5</sub> interannual variability during August–September in the Pacific Northwest (Fig.1c), with air stagnation index being the second most important predictor (11%), consistent with our prior work suggesting that air stagnation played an important role in the accumulation of PM<sub>2.5</sub> during the historic 2017 and 2018 fire seasons (11). The contributions from relative humidity, temperature, and precipitation are each less than 10%. A larger increase in correlation ( $r^2$ ) with meteorology is found in July and October than August or September, suggesting a more important role of meteorology in controlling PM<sub>2.5</sub> during these months (Fig.S1). These correlations confirm that it is important to consider impacts from both fires and meteorology for a robust estimation of changes in future PM<sub>2.5</sub> air quality.

We next examine the relationship between regional fires and PM<sub>2.5</sub> extremes defined as the 95<sup>th</sup> percentile (q95) of available daily PM<sub>2.5</sub> measurements from all sites within a 2°×2° grid for August and September (see *Methods* and Fig.S2). We still use monthly mean meteorological variables instead of extremes in the MLR model, since the q95 PM<sub>2.5</sub> in observations may not coincide with days having extreme meteorological conditions (i.e., heat wave, stagnation) and there are larger uncertainties in the predicted climate extremes than mean states. Significant correlations are observed between fire CO<sub>2</sub> emissions and the q95 PM<sub>2.5</sub> at most western US sites in August and September, based on simple linear

regression ( $r^2 = 0.5\text{--}0.9$ ; [Fig.1d](#)) and MLR ( $r^2 = 0.7\text{--}0.9$ ; [Fig.1e](#)). Fire CO<sub>2</sub> emissions explain 70% of the observed PM<sub>2.5</sub> interannual variability on average at US Pacific Northwest sites ([Fig.1f](#)), dominating over meteorological impacts.

The interannual variability of both mean and q95 PM<sub>2.5</sub> during August–September averaged over US Pacific Northwest sites shows a strong correlation ( $r^2 = 0.8\text{--}0.9$ ) with regional total fire CO<sub>2</sub> emissions over western North America ([Fig.1g-h](#)). In the 2017, 2018, and 2020 fire seasons, the western US experienced record-breaking wildfires burning ~50% more than the average area over the past two decades (54-56). The q95 PM<sub>2.5</sub> averaged over the US Pacific Northwest sites during August–September was 76 µg/m<sup>3</sup> in 2017, 44 µg/m<sup>3</sup> in 2018, and 95 µg/m<sup>3</sup> in 2020, respectively, exceeding the US National Ambient Air Quality Standard of 35 µg/m<sup>3</sup>.

These MLR analyses demonstrate significant interannual correlations of surface PM<sub>2.5</sub> pollution with regional fire CO<sub>2</sub> emissions and meteorology over the western US during August–September. Cross validation further confirms the robustness of the MLR model in predicting PM<sub>2.5</sub> ([SI Appendix, Text S1](#)). We obtain regression coefficients for the MLR model using the relationships of PM<sub>2.5</sub>, fires, and meteorological conditions observed in August–September during the period 1997–2020. Then we drive the MLR model with the monthly time series of fire CO<sub>2</sub> emissions and meteorological variables simulated by CMIP6 Earth system models under different climate change scenarios to predict PM<sub>2.5</sub> throughout the 21<sup>st</sup> century (see *Methods*).

### **Evaluating variability of fires simulated by CMIP6 models**

[\[Figure 2 about here\]](#)

To establish the robustness of future projections, we examine how well three CMIP6 models, the Community Earth System Model version 2 (CESM2) (57), the Geophysical Fluid Dynamics Laboratory Earth System Model version 4.1 (GFDL-ESM4.1) (58) and the Centre National de Recherches Météorologiques Earth System Model version 2 (CNRM-ESM2-1) (59), simulate historical fires. We use satellite observations of burned area from the MODerate Resolution Imaging Spectrometer (MODIS) (60) and satellite-based estimates of fire CO<sub>2</sub> emissions from the Global Fire Emissions Database (GFED4s) (61, 62) and the Quick Fire Emissions Dataset (QFED2.5) (63). Observations show hotspots of burned area and fire CO<sub>2</sub> emissions over the Pacific Northwest in August and

September (Fig.2a-b). We investigate the extent to which models capture the interannual variability of fires over this region relative to their respective mean state. Evaluating normalized interannual variability provides insights into the sensitivity of simulated fires to meteorological and climatic variability, which is critical to establish the robustness of projected fire responses to climate change.

We first examine the land-only experiments (see *Methods*) driven by observation-based meteorological forcings to allow direct comparison with the observed fires in space and time. The land-only simulations generally capture the observed normalized interannual variability of burned area ( $r^2 = 0.32$ – $0.67$ ) and fire CO<sub>2</sub> emission ( $r^2 = 0.25$ – $0.60$ ) over western North America (Fig.2c-d), despite mean-state biases (Fig.S3). Above-normal fire activity is observed and simulated in years such as 1988, 2006, 2012, 2017, 2018, and 2020, associated with severe drought conditions (64–69). The CESM2 model performs best in simulating the interannual variability of burned area ( $r^2 = 0.67$ ;  $p < 0.01$ ) and fire CO<sub>2</sub> emission ( $r^2 = 0.60$ – $0.64$ ;  $p < 0.01$ ). For comparison, the correlations for burned area are  $r^2 = 0.49$  ( $p < 0.01$ ) for CNRM-ESM2-1, and  $r^2 = 0.32$  ( $p < 0.05$ ) for GFDL-ESM4.1. The amplitude of the observed interannual variability of fire CO<sub>2</sub> emissions (represented as standard deviation in Fig.2) is also best captured by CESM2: s.d. = 36.4%, compared to s.d. = 55.9–56.2% in observations, s.d. = 28.3% in GFDL-ESM4.1, and 20.6% in CNRM-ESM2-1.

The fully coupled ocean-land-atmosphere experiments allow us to project future fires under varying climate change scenarios. These coupled model simulations are driven by model-generated climate and thus are not expected to capture the timing and location of the observed fires during historical periods. Therefore, we evaluate the hemispheric to regional patterns in burned area and fire CO<sub>2</sub> emissions, as well as the strength of interannual variability during the 1997–2014 period. Both the land-only and coupled experiments from all three models simulate the salient features of the spatial patterns of fire burned area and CO<sub>2</sub> emissions across the Northern Hemisphere, such as capturing fire hotspots over western North America and Mediterranean Europe in August and September (Figs.S4–S7). The models simulate reasonable fire interannual variability over these hotspots areas, despite large mean-state biases. Over western North America, total fire CO<sub>2</sub> emissions in August and September are overestimated by a factor of two in CESM2, and factors of 4–5 in GFDL-ESM4.1 and CNRM-ESM2-1, compared to the estimates from two satellite-based fire emission inventories (Fig.S3b). Similar high biases have previously been identified in CMIP5 Earth system models (23, 41) and by the CMIP6 Fire



Model Intercomparison Project (40). These studies suggest possible biases in the simulated fuel load (biomass), fire response to human activities, and fuel consumption rate applied in the models (40, 41, 70).

We conclude that the three CMIP6 Earth system models have moderate ability to simulate changes in fire emissions in response to variations in climate and vegetation, despite varying levels of mean-state biases. To gauge the uncertainties of our  $PM_{2.5}$  predictions associated with these biases, we compare MLR predictions driven by the relative changes of fire  $CO_2$  emissions versus those driven by the absolute emission changes in each model. For CESM2, with small mean-state biases in historical fire  $CO_2$  emissions, we find an overall consistent magnitude of western US mean  $PM_{2.5}$  predictions between the two MLR models (top panels in [Fig.S8](#)). For GFDL-ESM4.1 and CNRM-ESM2-1, with high mean-state biases in historical fire  $CO_2$  emissions, the MLR model driven by the absolute changes of fire emissions predicts much larger  $PM_{2.5}$  in 2080–2020, with the  $PM_{2.5}$  prediction driven by relative changes agreeing better with that driven by the CESM2 model (bottom panels in [Fig.S8](#)). Thus, we conclude that it is more reasonable to use the relative change of fire  $CO_2$  emissions to drive the MLR prediction of future  $PM_{2.5}$  levels.

### **Changes in climate and fires in the 21<sup>st</sup> century**

[\[Figure 3 about here\]](#)

We next investigate changes in climate and fires over western North America in the 21<sup>st</sup> century from the CMIP6 coupled Earth system simulations under four climate change scenarios: SSP1-2.6 (low societal vulnerability combined with radiative forcing of  $2.6 \text{ W m}^{-2}$  by 2100), SSP2-4.5 (intermediate societal vulnerability,  $4.5 \text{ W m}^{-2}$  forcing), SSP3-7.0 (high societal vulnerability,  $7.0 \text{ W m}^{-2}$  forcing) and SSP5-8.5 (fossil-fueled development, high emissions,  $8.5 \text{ W m}^{-2}$  forcing) (71, 72). While studies have suggested that fire seasonality may change in a warming climate (73-75), our MLR model predictions build upon the strong correlation between  $PM_{2.5}$  and fires during August–September over the Pacific Northwest under present-day climate. To investigate whether it is reasonable to focus on August–

September under future climate, we examine fire seasonality and spatial pattern over North America under SSP5-8.5 (Fig.3).

All three models project a lengthening of the fire season over the Pacific Northwest in a warmer climate, with elevated fire CO<sub>2</sub> emissions spanning from May to November during 2080–2100 under SSP5-8.5 compared to July to October at present (Fig.3a). Nevertheless, all three models suggest fire CO<sub>2</sub> emissions in the late 21<sup>st</sup> century peak in August and September, similar to the current climate. Therefore, we continue to focus our projections on changes in fires and PM<sub>2.5</sub> air quality in August and September. During August and September, fire CO<sub>2</sub> emissions are projected to increase significantly ( $p < 0.05$ ) over western North America (Fig.3b) and Mediterranean Europe (Figs.S9-S10) in the late 21<sup>st</sup> century under SSP5-8.5, according to our multi-ensemble and multi-model projections. These regions are particularly susceptible to water scarcity in a warming climate (76, 77), which could impact regional air quality via vegetation feedbacks (78).

[Figure 4 about here]

Figure 4 illustrates the temporal evolution of surface temperature, soil moisture, vegetation carbon mass, burned area, and fire CO<sub>2</sub> emissions from CESM2, which best simulates the observed interannual variability of fires, as discussed previously (Fig.2). Changes in fire CO<sub>2</sub> emissions and burned area from the other two models are also shown for comparison. CESM2 projects a ~2K increase in August–September mean surface temperature over western North America by the 2040s (versus present day), with little difference across the SSPs (Fig.4a). Surface temperatures among scenarios diverge afterwards, with a 7.5K increase under SSP5-8.5 compared to a 2K increase under SSP1-2.6 by the late 21<sup>st</sup> century (versus present day). Following climate warming and rising CO<sub>2</sub> concentrations, which stimulates vegetation growth, CESM2 simulates a decrease in surface soil moisture and an increase in vegetation carbon mass (Fig.4b-c), both providing more favorable conditions for fires. Under the SSP3-7.0 and SSP5-8.5 high-warming scenarios, CESM2 projects a ~10% decrease in surface soil moisture by the end of the 21<sup>st</sup> century. The projected decrease is consistent with the overall drying trend projected by 13 CMIP6 models (79), attributed primarily to enhanced evaporative demand and water use by vegetation in a warmer climate (80). Vegetation carbon mass shows a ~50% increase by

2100 under SSP5-8.5, partly driven by CO<sub>2</sub> fertilization, increased temperature, and land use changes (81-83).

Following the projected trends in climate and vegetation, CESM2 shows 50–120% increases in burned area and 110–250% increases in fire CO<sub>2</sub> emissions among different SSPs by 2100 over western North America (Fig.4d,g; Table S2). The different increases in fires among the scenarios reflect impacts from both climate and population distributions (37). The projected increases in fire CO<sub>2</sub> emissions are ~250% under the SSP3-7.0 and SSP5-8.5 extreme warming scenarios, more than twice that under the SSP1-2.6 climate mitigation scenario. We note a smaller increase in fire burned area under SSP5-8.5 (100%) compared to SSP3-7.0 (120%) (red versus yellow lines in Fig.4g). This may be related to the larger population projected under SSP5-8.5 (84) and thus stronger effects of fire suppression (85, 86). The influence of population density on fire suppression is also evident in historical simulations (Fig.S11). Across all scenarios, the projected increases in fire CO<sub>2</sub> emissions are about twice those in burned area (Fig.4), indicating increased emission efficiency per area burned driven partly by increased vegetation biomass or increased fire duration in a warming climate.

All three models project substantial increases in burned area and fire CO<sub>2</sub> emissions in the late 21<sup>st</sup> century, although the magnitudes of the projected changes, the spatial patterns, and the spreads across scenarios and across ensemble members differ (Fig.4 and Figs.S9-S10). The projected percentage increase in fire CO<sub>2</sub> emissions per degree warming is ~40% in CESM2 and GFDL-ESM4.1 and ~20% in CNRM-ESM2-1. Under SSP5-8.5 by the late 2100s, the projected increase in fire CO<sub>2</sub> emissions over western North America is 260% from GFDL-ESM4.1, 240% from CESM2, and 130% from CNRM-ESM2-1 (Fig.4d-f). GFDL-ESM4.1 shows the largest cross-scenario spread, with a 70% increase in fire CO<sub>2</sub> emissions under SSP1-2.6 and a 260% increase under SSP5-8.5 by the late 21<sup>st</sup> century (Fig.4e). Among the three models, CNRM-ESM2-1 has the simplest fire module but has the greatest number of ensembles (see *Methods and Table S1*). The larger ensemble spread for both historical and future simulations in CNRM-ESM2-1 results in a better estimate of the influence of the internal climate variability on fire emissions. There are also some inter-model differences in the spatial distribution of the projected fire increases over western North America (Figs.S9-S10). CESM2 shows larger increases of fire burned area and emissions over the northern Great Plains, while CNRM-ESM2-1 and GFDL-

ESM4.1 simulate larger increases over the Pacific Northwest. These results highlight the importance of multi-model and multi-ensemble projections to assess uncertainties.

### **Comparison with previous studies**

A few prior studies have estimated changes in fire emissions in the 21<sup>st</sup> century. Here we present a brief comparison with our results. Under SSP2-4.5 by midcentury, the three CMIP6 models we consider projected a 60–80% increase in fire emissions over western North America. Our projected changes are smaller than the ~150% increase projected by a statistical fire model considering impacts from climate but not land use and population density (26). This is consistent with the smaller increase in fire carbon emissions over western North America during 1960s–2010s from the CESM2 coupled historical simulations using interannually varying versus fixed-1850 land use and population density (Fig.S11). Increased population density leads to greater fire suppression, wood harvest, and conversion of natural land (i.e. forest) to managed land (i.e. cropland), resulting in reduced forest biomass available for burning (40, 43, 87). Our projection of 60–80% increase in fire CO<sub>2</sub> emissions over western North America is higher than the 45% increase projected by an offline process-based fire model driven by archived meteorological fields (23). The larger changes from our projection may be related to a positive feedback between fire and climate, e.g. increased fire risk due to enhanced surface temperature caused by fire-induced damage in vegetation canopy, which is not included in the offline simulation (37, 42, 88). The comparisons suggest that it is important to consider the impacts from climate, land use, and population influence for a robust projection of fires and feedbacks.

### **Increasing PM<sub>2.5</sub> pollution from wildfires in a warming climate**

[\[Figure 5 about here\]](#)

Changes in fire CO<sub>2</sub> emissions and meteorology projected by three CMIP6 Earth system models are used to drive the MLR model to predict PM<sub>2.5</sub> over the western US under four SSP scenarios (Fig.5, Table S2). The MLR model driven by historical fires generally captures the observed variability and increasing trend of western US PM<sub>2.5</sub> in August–September during 1997–2020, demonstrating the credibility of the MLR-based PM<sub>2.5</sub> estimations (red versus black lines in Fig.5d-f). The MLR model driven by simulated future fires projects August–September mean PM<sub>2.5</sub> levels at western US sites to increase by approximately 50% in the coming decades (2020–2050), even under the SSP1-2.6 strong-mitigation scenario with global CO<sub>2</sub> emissions cut severely and reaching net-zero around 2050. Under

the “middle-of-the-road” SSP2-4.5 scenario, CO<sub>2</sub> emissions hover around current levels before falling mid-century, but do not reach net-zero by 2100 (71, 72); wildfire emissions and resulting PM<sub>2.5</sub> pollution would continue to increase after 2050 and almost double by 2100 compared to present-day levels (green lines in Figs.4d-f and 5d-f). Under SSP5-8.5, with CO<sub>2</sub> emissions roughly double present levels by 2050 (71, 72) and western US summer mean temperature rising 6–8 K by the end of the century (Fig.4a), mean PM<sub>2.5</sub> levels resulting from increasing wildfires during August–September could double to triple compared to present-day levels (red lines in Fig. 5d-f), reaching 15–45 µg/m<sup>3</sup> for the US Pacific Northwest and northern California by the late 21<sup>st</sup> century (Fig.5a-c; Table S2). These PM<sub>2.5</sub> increases are primarily driven by marked increases in fire emissions in the warming climate (Fig.S12), with a small contribution from increasing stagnation frequency (Fig.S13).

In contrast, PM<sub>2.5</sub> simulated directly by chemistry-climate models, using prescribed fire emissions of aerosol precursors responding to changes in land use but not climate (see *Methods*), do not show significant changes (+7%) throughout the 21<sup>st</sup> century under SSP5-8.5 (tan lines in Fig.5d-f). The prescribed fire emissions show little trend over western North America during the 21<sup>st</sup> century (Fig.S14). The minor changes in anthropogenic emissions from the combustion of fossil fuels over western North America are not accounted for in our MLR PM<sub>2.5</sub> predictions.

[Figure 6 about here]

We next examine changes in PM<sub>2.5</sub> extremes predicted by our MLR model in response to enhanced fire activity under the intermediate-mitigation SSP2-4.5 and low-mitigation SSP5-8.5 scenarios (Fig.6). We predict considerable deterioration of PM<sub>2.5</sub> air quality over the western US in the 21<sup>st</sup> century under SSP5-8.5, caused by fires. By 2080–2100 under SSP5-8.5, the q95 of daily PM<sub>2.5</sub> in August–September is 20–170 µg/m<sup>3</sup> at Pacific Northwest sites, with 72–96% (model spread) of the sites experiencing q95 PM<sub>2.5</sub> above the 35 µg/m<sup>3</sup> US national standard, 52–68% above the unhealthy level (55 µg/m<sup>3</sup>), and 0–8% above the very unhealthy level (150 µg/m<sup>3</sup>; Fig.6a-c). The q95 PM<sub>2.5</sub> in August–September averaged over US Pacific Northwest sites exceeds the 35 µg/m<sup>3</sup> US national standard by mid-21<sup>st</sup> century under both SSP2-4.5 and SSP5-8.5 (Fig.6d-f). By the late 21<sup>st</sup> century, the estimated q95 PM<sub>2.5</sub>

levels averaged over US Pacific Northwest sites in individual models and ensembles could reach as much as 85–125  $\mu\text{g}/\text{m}^3$  under SSP2-4.5 and 115–155  $\mu\text{g}/\text{m}^3$  under SSP5-8.5.

[\[Figure 7 about here\]](#)

Large fires burning across the US West in 2017, 2018, 2020, and 2021 caused historic levels of air pollution, loss of human life, and property damage (12, 54, 56). Unhealthy to hazardous concentrations of  $\text{PM}_{2.5}$  (55–500  $\mu\text{g}/\text{m}^3$ ) were recorded at sites in the US Pacific Northwest and California for extended periods during summer to fall (11, 12). We use extreme value theory to examine whether these historically consequential events are more likely to occur in a future climate under intermediate and high emissions scenarios (*Methods*). We analyze large samples of q95  $\text{PM}_{2.5}$  at each site over the US Pacific Northwest during August–September from historical extremes (2017, 2018, and 2020), all historical observations for 1997–2020, and the MLR projections for 2080–2100 (*Fig.7*). We find that the shape of the exceedance probability distribution of q95  $\text{PM}_{2.5}$  during the late 21<sup>st</sup> century under SSP5-8.5 resembles that for the historic  $\text{PM}_{2.5}$  extremes of 2017, 2018, and 2020 caused by fires: ~70% of sites have q95  $\text{PM}_{2.5}$  exceeding the 35  $\mu\text{g}/\text{m}^3$  US national standard, compared to only 16% for average conditions observed during the past two decades (*Fig.7a*). Under SSP2-4.5, the  $\text{PM}_{2.5}$  distribution also shows a substantial shift towards extreme conditions. *Figure 7b* shows the return period of the q95  $\text{PM}_{2.5}$  at US Pacific Northwest sites, fitted using a generalized extreme value distribution, from historical observations and the MLR  $\text{PM}_{2.5}$  predictions. For a range of return periods (e.g., 5, 10, 20 years), the estimated q95  $\text{PM}_{2.5}$  would double to triple in the MLR projections compared with historical observations. The return period of the recent pollution extremes of 2017, 2018, and 2020 (with a mean August–September q95  $\text{PM}_{2.5}$  of 72  $\mu\text{g}/\text{m}^3$ ) would decrease to approximately 5 years in the late 21<sup>st</sup> century under SSP2-4.5 and to 3 years under SSP5-8.5.

## Conclusions and Implications

Using an empirical statistical model driven by observations and CMIP6 Earth system model projections of fire  $\text{CO}_2$  emissions and meteorology, we project western US  $\text{PM}_{2.5}$  air quality in the 21<sup>st</sup> century under a suite of Shared Socioeconomic Pathways (SSPs). Late summer to fall  $\text{PM}_{2.5}$  pollution over the US Pacific Northwest is projected to double to triple by 2080–2100 due to enhanced fire activity associated with drought and increased biomass under intermediate (SSP2-4.5) and high warming scenarios (SSP5-8.5). Even with strong mitigation under SSP1-2.6, western US  $\text{PM}_{2.5}$

pollution would increase ~50% by mid-century. The occurrence of four severe fire years in quick succession during 2017–2021 over the western US raises the possibility that climate change is already driving strong changes in fire regimes that may be underestimated by our models. Our study suggests that severe PM<sub>2.5</sub> air pollution caused by these historic fire events could occur every 5 years in the late 21<sup>st</sup> century under an intermediate climate change scenario (SSP2-4.5). Air quality exceedances caused by wildfires can be classified as 'exceptional events,' which are not counted towards a non-attainment determination, according to the US Environmental Protection Agency. However, a considerable increase in the frequency of fire-driven exceedances may complicate this policy, as these events become a new norm in the changing climate. The large spread across climate change scenarios highlights the co-benefits of climate mitigation for wildfires and air pollution. Multi-agency collaborations, addressing climate mitigation, air quality, and forest management, are needed to minimize the adverse health impacts projected to result from fire smoke.

## Materials and Methods

### 1. Data availability

The data from three CMIP6 models used in this study (89-91) are publicly available at <https://esgf-node.llnl.gov/projects/cmip6/>. Surface observations of PM<sub>2.5</sub>, meteorological variables from reanalysis datasets, satellite observations of burned area, and fire emission inventories are publicly available through the links provided at the corresponding references as described below.

### 2. Multi-linear regression model

The multiple linear regression (MLR) model is developed using observational datasets of surface PM<sub>2.5</sub> concentrations, meteorological variables, and fire CO<sub>2</sub> emissions over western North America during 1997–2020. This observation-based MLR model is then applied to predict future PM<sub>2.5</sub> levels driven by fire CO<sub>2</sub> emissions and meteorology projected by the CMIP6 Earth system models. Considering that climate model projections are more robust on larger scales, all observational datasets and CMIP6 model fields used for the MLR analysis are averaged onto a 2°×2° grid. The MLR model predicts the mean and the 95<sup>th</sup> percentile of PM<sub>2.5</sub> at each 2°×2° grid *d* and month *i* in the form of:

$$PM_{2.5,d,i}(t) = \beta_{d,i} Fire_{d,i}(t) + \sum_{k=1}^4 \beta_{d,i,k} Met_{d,i,k}(t) + b_{d,i} \quad (1)$$

where  $\text{Fire}(t)$  is the anomaly time series of fire  $\text{CO}_2$  emissions in percentage relative to the present-day climatology,  $\text{Met}(t)$  is the anomaly time series of meteorological variables (i.e., surface temperature, precipitation, relative humidity, and air stagnation) relative to the present-day climatology;  $\beta$  and  $b$  are regression coefficients fitted by the MLR. We select these four meteorological variables that have been previously identified to be correlated with surface  $\text{PM}_{2.5}$  (11, 52). We performed the regression by adding and deleting prediction parameters stepwise to obtain the best fit based on the Akaike Information Criterion. The relative importance of each predictor is determined using a bootstrap approach described in (92). The performance of the MLR model is tested using leave-one-out cross-validation (*SI Appendix, Text S1*).

The observation-based MLR model is applied to predict mean and the 95<sup>th</sup> percentile of surface  $\text{PM}_{2.5}$  concentrations at each  $2^\circ \times 2^\circ$  grid, driven by monthly time series of fire  $\text{CO}_2$  emissions and meteorology projected by the CMIP6 Earth system models under a suite of climate change scenarios over the course of the 21<sup>st</sup> century. To ensure that we only apply the MLR predictions at locations where  $\text{PM}_{2.5}$  levels are primarily driven by fire emissions, we limit our analysis to western US grid cells where the observed correlation  $r^2$  from the MLR model is greater than 0.5 during August and September; as such, sites located in urban areas with large anthropogenic influence are filtered out. For  $\text{PM}_{2.5}$  prediction at each valid grid, we calculate the anomaly time series (in percentage relative to the present-day 1990–2010 climatology) of total fire  $\text{CO}_2$  emissions in a projected future climate, integrated over a regional box where the maximum correlation with  $\text{PM}_{2.5}$  is found based on historical observations (*Fig.1*). This approach thus accounts for the influence of regional smoke transport. Anomaly time series of meteorological variables in the future climate are calculated as the absolute differences from the present-day 1990–2010 climatology for each valid  $2^\circ \times 2^\circ$  grid.

### 3. Observational datasets

Daily observations of  $\text{PM}_{2.5}$  at surface monitoring sites during 1997–2020 are obtained from the US Environmental Protection Agency's Air Quality System (<https://www.epa.gov/aqs>). To maximize data availability, we include  $\text{PM}_{2.5}$  measured with both the Federal Reference Methods and non-Federal Reference Methods, as a strong linear correlation ( $r^2=0.92$ ) between these two methods has been found at co-located monitors (93). To be consistent with the other datasets used for the MLR analysis



as well as to increase the statistical power and robustness of the analysis, we average all available daily surface PM<sub>2.5</sub> observations onto a 2°x2° grid. For each month at each 2°x2° grid cell, we calculate the average and the 95<sup>th</sup> percentile of available daily PM<sub>2.5</sub> from all sites within that grid. Most grids have sample sizes of 50–200 daily PM<sub>2.5</sub> observations each month; only grids with at least 20 samples per month are considered in our analyses ([Fig.S2](#)).

To represent the intensity and severity of wildfires, we use satellite observations of burned area and satellite-based estimations of fire CO<sub>2</sub> emissions, consistent with the datasets available from the CMIP6 fire models. The monthly burned area is from the Collection 6 Moderate Resolution Imaging Spectrometer (MODIS) climate model grid burned area product (2000–2020, 0.25°x0.25°) (60). Fire emissions of CO<sub>2</sub> are obtained from the Global Fire Emissions Dataset version 4 with small fires (GFED4s, 1997–2020, 0.25°x0.25°) based on satellite-retrieved burned area (61, 62), and the Quick Fire Emission Dataset version 2.5 (QFED2.5, 2001–2019, 0.1°x0.1°) based on satellite-observed fire radiative power (63). The MLR model only uses fire CO<sub>2</sub> emissions from GFED4s averaged onto a 2.0x2.0 grid while both GFED4s and QFED2.5 are used to evaluate the CMIP6 fire models.

The MLR analysis includes four meteorological variables that have been previously identified to have correlations with surface PM<sub>2.5</sub> (11, 52): surface temperature, precipitation, relative humidity, and air stagnation ([SI Appendix, Text S2](#)). Monthly mean surface temperature, precipitation and relative humidity are obtained from the European Centre for Medium-Range Weather Forecasts Reanalysis version 5 (ERA5, 1997–2020, 0.1°x0.1°) (94). The air stagnation index is obtained from the U.S. National Centers for Environmental Information (95). All original datasets are averaged onto a 2°x2° grid for the MLR analysis.

#### **4. CMIP6 Fire Models**

We use simulations from three CMIP6 Earth system models (CESM2, GFDL-ESM4.1 and CNRM-ESM2-1) that archived CO<sub>2</sub> emissions from fires and meteorological variables needed for the MLR model. The models' horizontal resolutions range from 1.0 to 1.5° ([Table S1](#)). Vegetation structure and functioning in all three models (e.g., leaf area index) respond to changes in climate. GFDL-ESM4.1 simulates daily vegetation distribution (58, 96-98) while CESM2 and CNRM-ESM2-1 use prescribed land use and land cover change files (49, 59). Fire CO<sub>2</sub> emissions in all three CMIP6 models are simulated dynamically, coupled to climate and vegetation ([SI Appendix, Text S3](#)) (42, 43, 45-47, 50,

51, 99). However, these models do not calculate fire emissions of particles or non-CO<sub>2</sub> gases, so atmospheric chemistry in these models is not coupled to interactive fire emissions responding to climate change.

Two sets of experiments from these models are used: (1) Land-only experiments (LAND-HIST experiment from the Land Use Model Intercomparison) driven by the observation-based meteorological forcings (derived from dynamic downscaling of the 20<sup>th</sup>-Century Reanalysis) (100, 101); (2) Coupled land-atmosphere-ocean historical simulations (CMIP6 HIST experiment) and future projections (from the Scenario Model Intercomparison Project) driven by emissions of greenhouse gases and aerosols under four Shared Socioeconomic Pathways: SSP1-2.6, SSP2-4.5, SSP3-7.0, SSP5-8.5 (71). The land-only experiments driven by observed climate allow for direct comparison with observations in space and time in order to understand biases related to the modeling of fire dynamics (Fig.2). The coupled model simulations are used to understand changes in fires under climate change scenarios, which serve as a key predictor for future PM<sub>2.5</sub> levels (Figs.5-7). To understand the drivers of the temporal evolution of historical fires (Fig.S11), we analyze three CESM2 coupled-model experiments: (1) with all historical forcings (HIST); (2) the control simulation with pre-industrial forcings, including constant land cover and land use, land management, and population density at 1850 levels (pi-Control) (102); (3) with all historical forcings same as HIST but with land use held constant at 1850 levels as in pi-Control (HIST\_NoLU) (101).

## **5. Chemistry-climate model PM<sub>2.5</sub> simulations using prescribed fire emissions**

We compare the MLR-based estimations of PM<sub>2.5</sub> driven by interactive fires responding to climate change with PM<sub>2.5</sub> directly simulated by three chemistry-climate models (103-105). In these chemistry-climate models, fire emissions of particles are prescribed for both historical and future simulations. Historical simulations of these models use fire emissions of gases and particles from GFED version 4 with small fires (GFED4s) for 1997–2014, and historical reconstructions from the Fire Model Intercomparison project prior to 1997 (28, 48). Future fire emissions of gases and particles are prescribed based on the spatial distribution of the 2005–2014 climatology from GFED4s, and consider the impacts from land use but not climate change (29). There are no substantial trends nor interannual variability in biomass burning emissions of aerosols used for future PM<sub>2.5</sub> projections from

these chemistry-climate models (Fig.S14). Future PM<sub>2.5</sub> levels simulated by these chemistry-climate models thus reflect the impacts from changes in anthropogenic emissions and meteorology, but overlook the impact of climate-driven increases in fire emissions of aerosols and aerosol precursors.

## 6. Calculation of exceedance probability and return period

To examine how prevalent the recent PM<sub>2.5</sub> pollution extremes caused by fires in 2017, 2018 and 2020 may be in a warming climate, we compare the exceedance probability and return period of the 95<sup>th</sup> percentile (q95) of daily PM<sub>2.5</sub> in August–September at US Pacific Northwest sites from historical observations with MLR projections under SSP2-4.5 and SSP5-8.5 scenarios.

The exceedance probability is calculated as  $1-F_n$ , where  $F_n$  is the empirical cumulative distribution function, calculated as  $F_n(t) = \frac{1}{n} \sum_{i=1}^n \mathbf{1}_{X_i \leq t}$ , where  $n$  is the total number of the predicted monthly q95 PM<sub>2.5</sub> at each site in the US Pacific Northwest in August and September.  $\sum_{i=1}^n \mathbf{1}_{X_i \leq t}$  is the number of events with the predicted q95 PM<sub>2.5</sub> smaller than a given q95 PM<sub>2.5</sub> level of  $t$ .

The return levels and return periods are estimated using extreme value theory (106). Extreme value theory has been used in previous studies to estimate return levels and days of ozone pollution events under present and future climates (107-109). Here in this study, we perform the extreme event analysis with the extRemes package in R (110) using large samples of q95 PM<sub>2.5</sub> at each site in the US Pacific Northwest during August–September from historical extremes (2017, 2018, and 2020), from all historical observations for 1997–2020, and from the MLR projections for 2080–2100. The observed and MLR-predicted q95 PM<sub>2.5</sub> are fitted using a generalized extreme value distribution function. The 95% confidence intervals are estimated based on the delta method using the parameter covariance (110).

## Acknowledgments

This study was supported by awards from National Oceanic and Atmospheric Administration (NOAA), US Department of Commerce (NA14OAR4320106 and NA18OAR4320123). The statements, findings, conclusions, and recommendations are those of the authors and do not necessarily reflect the views of NOAA. RS acknowledges the European Union's Horizon 2020 research and innovation program under grant agreement No. 101003536 (ESM2025 – Earth System Models for the Future).

We thank Yan Yu, Songmiao Fan and Wenhao Dong from NOAA GFDL and two anonymous reviewers for their helpful comments on the manuscript.

**Figures:**

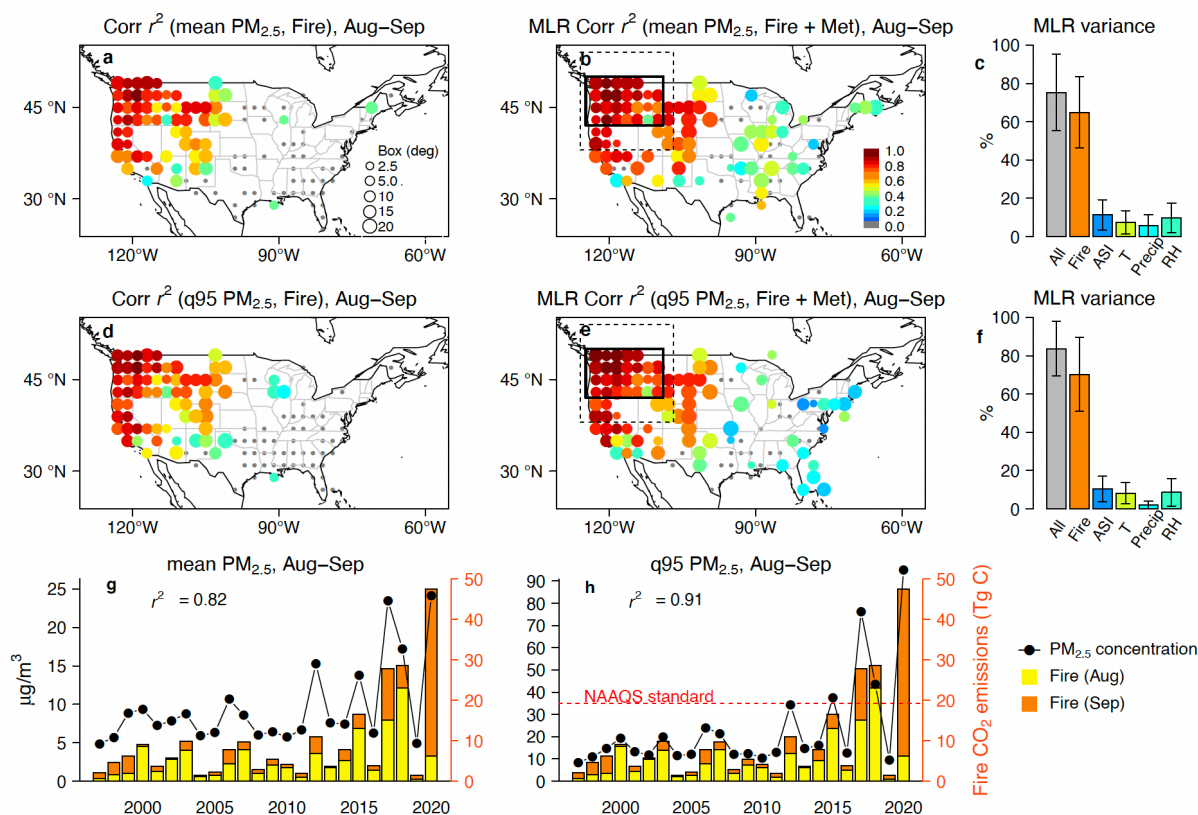


**Figure 1. Observed correlations between fires and surface PM<sub>2.5</sub> air quality.** (a–c) Correlation  $r^2$  of mean PM<sub>2.5</sub> averaged over each  $2^\circ \times 2^\circ$  grid with regional total CO<sub>2</sub> emissions from fires in August–September during 1997–2020 derived from simple linear regression (a) versus multiple linear regression (MLR) with consideration of meteorological variables (b), and the variance explained over the US Pacific Northwest (solid black box on b) by each predicting variable (c). The width of the box (in degrees), within which regional total fire emissions are best correlated with PM<sub>2.5</sub> at that site, is given in the right corner in (a). The  $r^2$  values are color-coded for sites with significant correlations, with gray indicating sites with insignificant correlations ( $p > 0.05$ ). (d–f) Same as (a–c) but for the 95<sup>th</sup> percentile (q95) of available daily PM<sub>2.5</sub> observations at each grid in August–September. (g–h) Time series of the mean and q95 PM<sub>2.5</sub> in August–September averaged over US Pacific Northwest sites from 1997 to 2020, along with regional total CO<sub>2</sub> emissions from fires integrated over western North America (dashed black box on b).

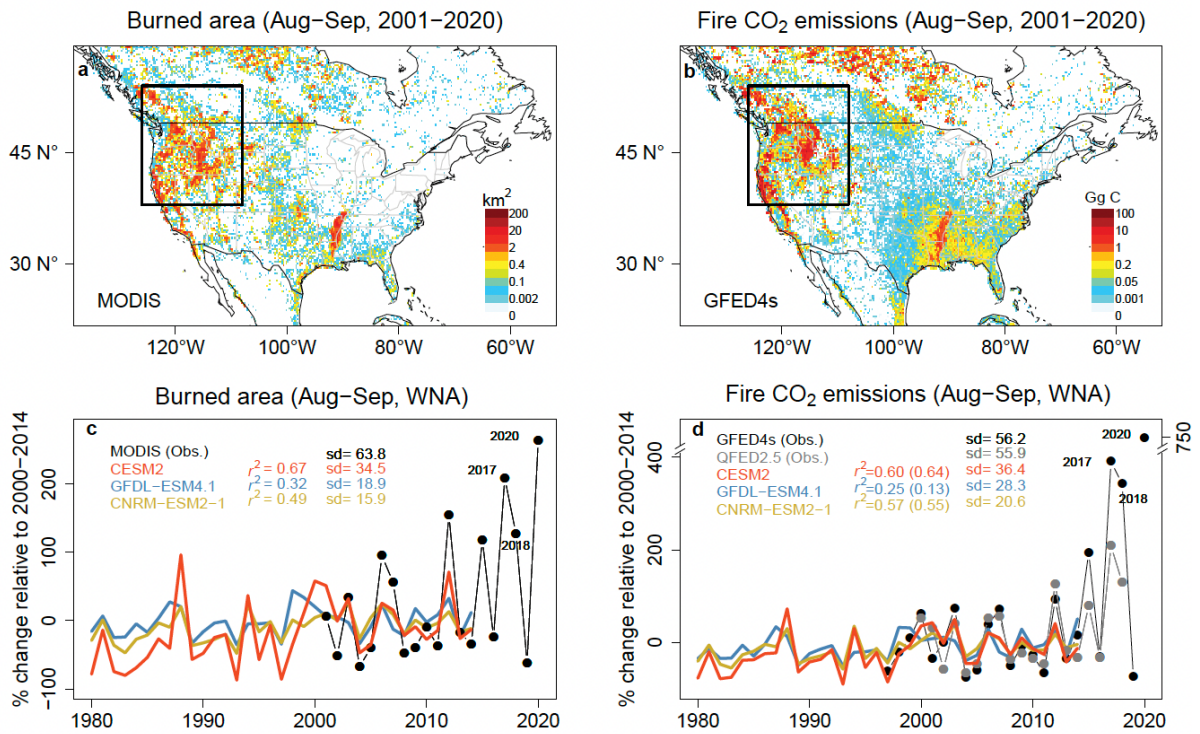


**Figure 2. Evaluating model simulations of fires over western North America.** (a-b) The 2001–2020 climatology of August–September total burned area from MODIS satellite observations and fire CO<sub>2</sub> emissions from GFED4s over North America. (c) The relative changes of August–September total burned area over western North America (WNA, black box on map) from 1980 to 2020 versus 2000–2014 averages from MODIS satellite observations (black) and from three CMIP6 land-only experiments (solid lines). (d) same as (c) but for fire CO<sub>2</sub> emissions from two satellite-based inventories (black for GFED4s and gray for QFED2.5) and from three CMIP6 land-only experiments (solid lines). Standard deviations (sd, in percentage) and correlations  $r^2$  between models and observational datasets (QFED2.5 in parentheses) are shown in c and d.

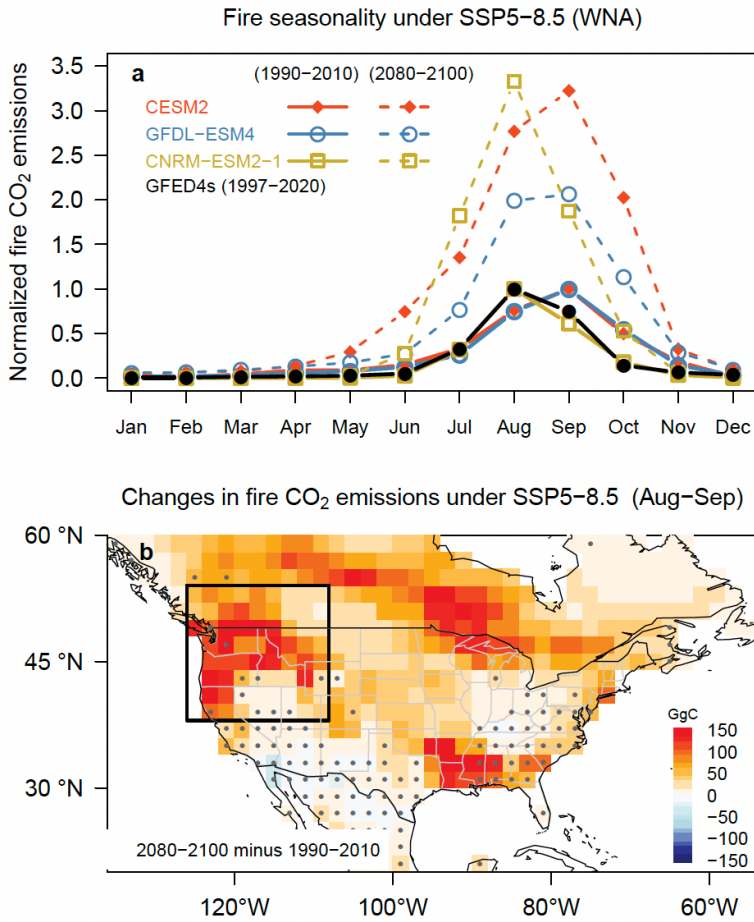


**Figure 3. Changes in fire seasonality in the late 21<sup>st</sup> century.** (a) Monthly mean fire CO<sub>2</sub> emissions over western North America under present day (1990–2010, solid lines) and SSP5-8.5 (2080–2100, dashed lines) normalized by the month with peak emissions at present day from CMIP6 coupled model experiments. Also shown are satellite-based estimates for present-day climate (black). (b) Multi-model and multi-ensemble mean changes in CO<sub>2</sub> emissions from fires (in Gg C) in August–September during the late 21<sup>st</sup> century under SSP5-8.5 (2080–2100 minus 1990–2010). The results are first averaged across the available ensemble members from each model (3 for CESM2, 1 for GFDL-ESM4.1, and 5 for CNRM-ESM2-1), and then averaged across the models. Stippling indicates grids with less than two models show statistically significant ( $p < 0.05$ ) changes or where the three models do not agree in sign. For each model, a change is defined significant if >50% of the ensemble changes are statistically significant ( $p < 0.05$ ).

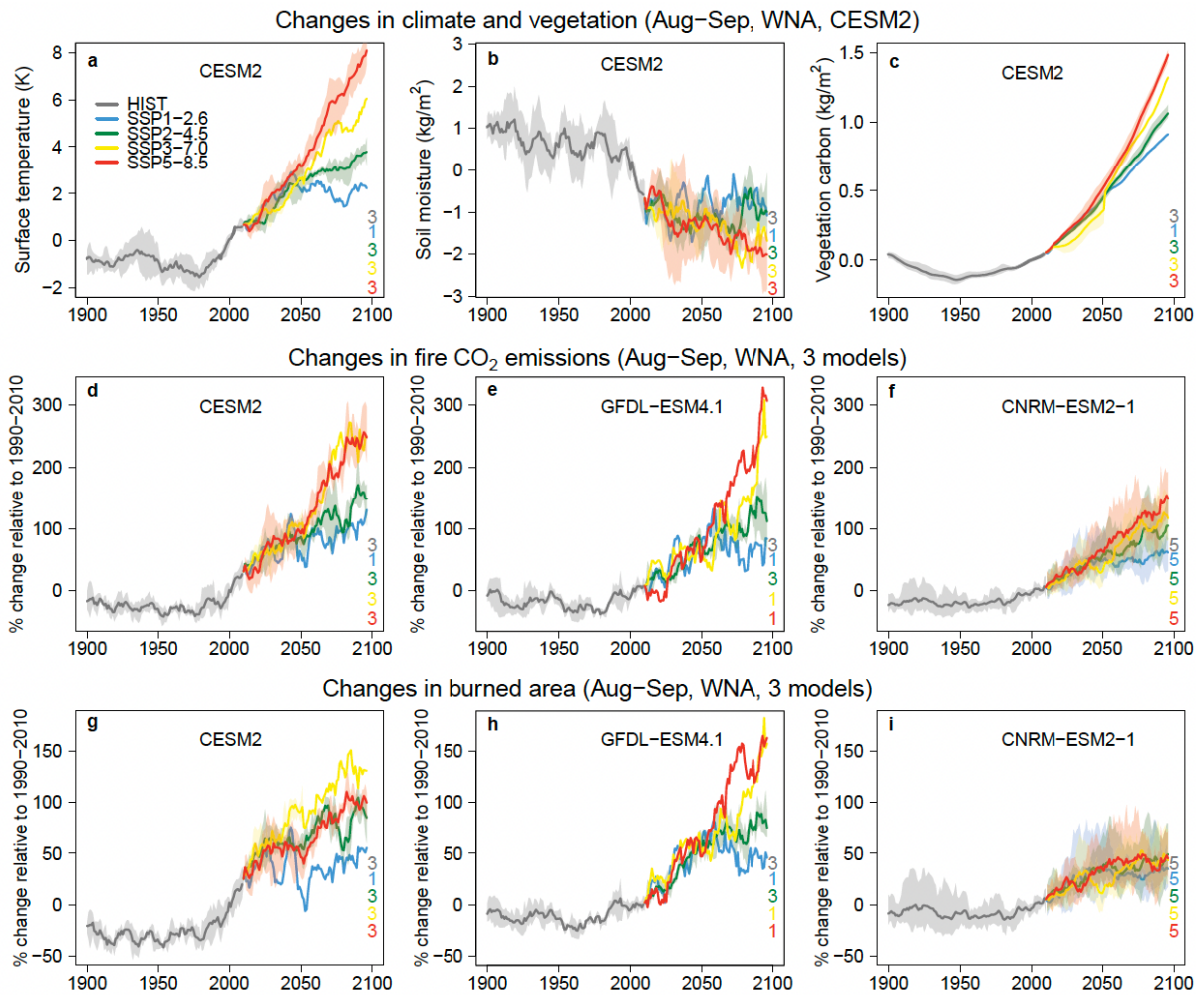


**Figure 4. Changes in climate and fires during August–September in the 21<sup>st</sup> century.** Changes in 10-year running average of surface temperature (a), soil moisture in top 10 cm (b), and carbon mass in vegetation (c) relative to the 1990–2010 averages in August–September over western North America from CESM2 historical simulations (gray) and future projections (colors) under four SSPs (Table S1). (d-f) same as (a) but for total fire emissions of CO<sub>2</sub> (in percent) and (g-i) burned area (in percent) from three CMIP6 Earth System models: CESM2 (left), GFDL-ESM4.1 (middle) and CNRM-ESM2-1 (right). Thick lines represent the multi-ensemble mean, with shading illustrating the spread of available ensemble members (numbers denoted at the bottom-right corner of each graph).



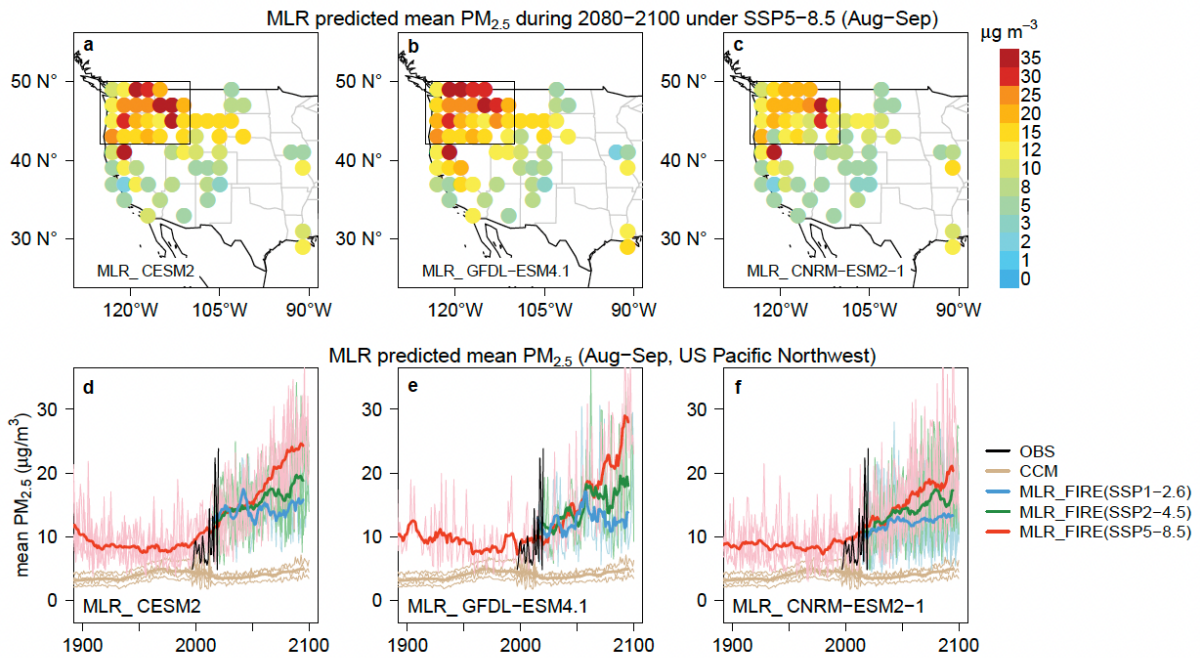


**Figure 5. Projected changes in August–September mean  $PM_{2.5}$  due to increasing fire emissions.** (a–c) The August–September mean  $PM_{2.5}$  in 2080–2100 at western US sites (averaged over a  $2^\circ \times 2^\circ$  grid) predicted by MLR driven by fires from three CMIP6 models under SSP5-8.5. Only grids with MLR correlation  $r^2 > 0.5$  are shown. (d–f) Temporal evolution of August–September mean  $PM_{2.5}$  averaged over US Pacific Northwest sites (box on map) during 1900–2100 from the chemistry-climate model simulations with prescribed fire emissions (tan lines) versus from the MLR model predictions considering the impacts of future climate change on fire emissions under SSP1-2.6 (blue lines), SSP2-4.5 (green lines), and SSP5-8.5 (red lines). Thick lines represent 10-year running multi-ensemble averages and thin lines represent averages for individual years from each ensemble member of each model (3 for CESM2, 1 for GFDL-ESM4.1, and 5 for CNRM-ESM2-1). The August–September interannual time series from observations (black lines) is also shown for comparison.

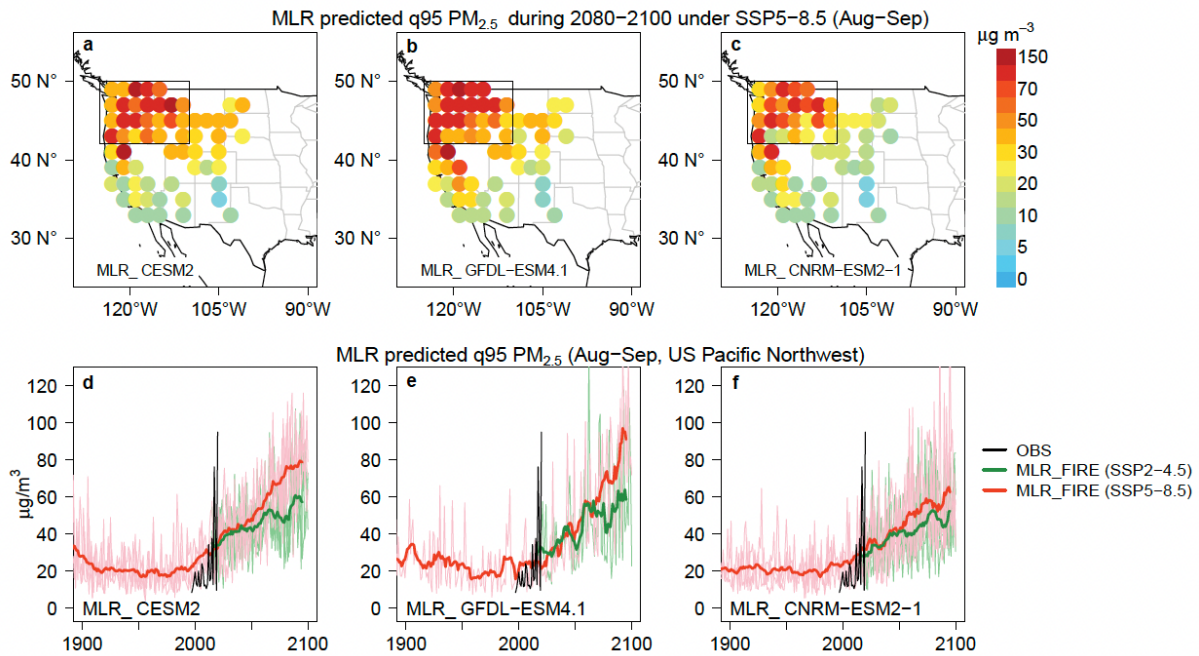


**Figure 6. Projected changes in  $PM_{2.5}$  extremes in August–September due to increasing fires.** (a-c) The 95<sup>th</sup> percentile of daily  $PM_{2.5}$  (q95) during August–September in 2080–2100 at western US sites (computed over a  $2^\circ \times 2^\circ$  grid) predicted by MLR driven by fires from three CMIP6 models under SSP5-8.5. Only grids with MLR correlation  $r^2 > 0.5$  are shown. (d-f) Temporal evolution of the q95  $PM_{2.5}$  in August–September averaged over US Pacific Northwest sites (box on map) from the MLR model projections under SSP2-4.5 (green) and SSP5-8.5 (red). Thick lines represent 10-year running multi-ensemble averages and thin lines represent averages for individual from each ensemble member of each model (Table S1). The August–September interannual time series from observations (black lines) is also shown for comparison.

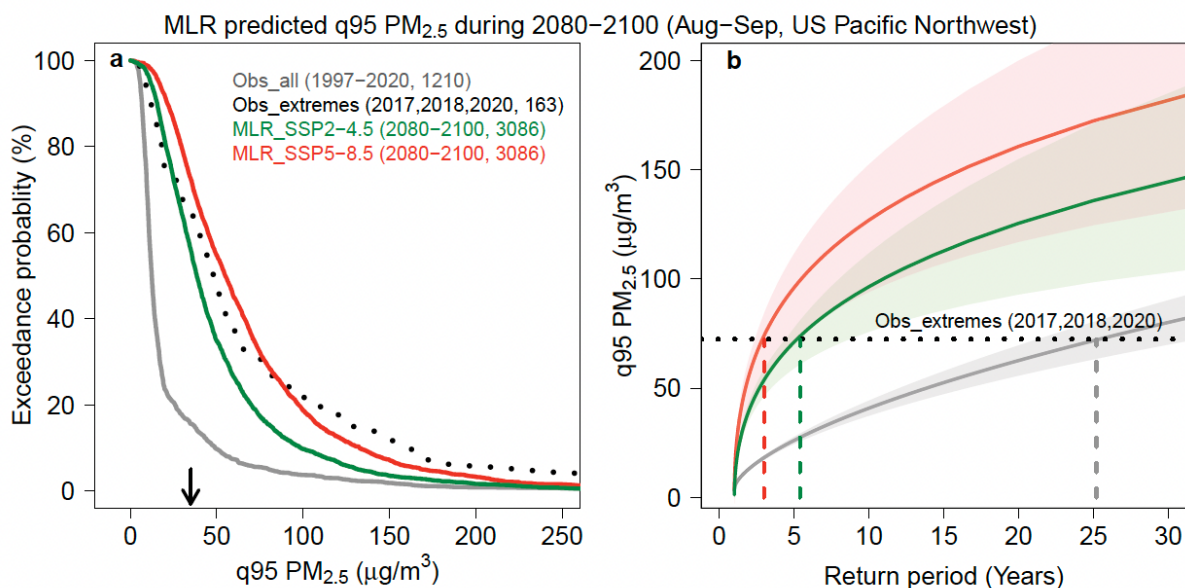


**Figure 7. Likelihood of historical pollution extremes in a warming climate.** Exceedance probability of the 95<sup>th</sup> percentile of daily PM<sub>2.5</sub> at US Pacific Northwest sites during August–September: from observations during 1988–2020 (gray solid line) and during the 2017, 2018 and 2020 extreme fire seasons (black dotted line), from the MLR PM<sub>2.5</sub> predictions driven by fires in three CMIP6 models during 2080–2100 under SSP2-4.5 (green) and SSP5-8.5 (red). The arrow denotes the 35 µg/m<sup>3</sup> US National Ambient Air Quality Standard for 24-h average PM<sub>2.5</sub>. Numbers in brackets represent sample size for calculating the exceedance probability; (b) return period of the 95<sup>th</sup> percentile of daily PM<sub>2.5</sub> at US Pacific Northwest sites in August–September fitted using generalized extreme value distribution: from observations during 1997–2020 (black solid line), and from the MLR PM<sub>2.5</sub> predictions driven by fires in three CMIP6 models during 2080–2100 under SSP2-4.5 (green) and SSP5-8.5 (red). The 95<sup>th</sup> percentile of daily PM<sub>2.5</sub> in August–September of 2017, 2018 and 2020 is marked as the horizontal dotted line. Shading for observations represents the 95% confidence intervals of estimated PM<sub>2.5</sub> levels for different return periods. Shading for MLR projections represents the maximum and minimum of estimated PM<sub>2.5</sub> levels for different return periods from different model ensembles. Intercepts between the horizontal black dotted line and the fitted solid lines represent the return periods for the observed 2017–2020 extremes in present and future climates.

## References

1. USEPA, Data from the 2017 National Emissions Inventory. <https://www.epa.gov/air-emissions-inventories/2017-national-emissions-inventory-nei-data> (2017).
2. D. M. J. S. Bowman *et al.*, Vegetation fires in the Anthropocene. *Nature Reviews Earth & Environment* **1**, 500-515 (2020).
3. F. H. Johnston *et al.*, Estimated Global Mortality Attributable to Smoke from Landscape Fires. *Environmental Health Perspectives* **120**, 695-701 (2012).
4. M. Burke *et al.*, The changing risk and burden of wildfire in the United States. *Proceedings of the National Academy of Sciences* **118**, e2011048118 (2021).
5. G. P. Schill *et al.*, Widespread biomass burning smoke throughout the remote troposphere. *Nature Geoscience* **13**, 422-427 (2020).
6. A. L. Westerling, H. G. Hidalgo, D. R. Cayan, T. W. Swetnam, Warming and earlier spring increase western US forest wildfire activity. *Science* **313**, 940-943 (2006).
7. A. L. Westerling, Increasing western US forest wildfire activity: sensitivity to changes in the timing of spring. *Philos Trans R Soc Lond B Biol Sci* **371** (2016).
8. J. T. Abatzoglou, A. P. Williams, Impact of anthropogenic climate change on wildfire across western US forests. *Proceedings of the National Academy of Sciences* **113**, 11770-11775 (2016).
9. C. D. McClure, D. A. Jaffe, US particulate matter air quality improves except in wildfire-prone areas. *Proceedings of the National Academy of Sciences* **115**, 7901-7906 (2018).
10. K. O'Dell, B. Ford, E. V. Fischer, J. R. Pierce, Contribution of Wildland-Fire Smoke to US PM<sub>2.5</sub> and Its Influence on Recent Trends. *Environmental Science & Technology* **53**, 1797-1804 (2019).
11. Y. Xie, M. Lin, L. W. Horowitz, Summer PM<sub>2.5</sub> pollution extremes caused by wildfires over the western United States during 2017–2018. *Geophysical Research Letters* **47**, e2020GL089429 (2020).
12. R. J. Laing, D. A. Jaffe, Wildfires are causing extreme PM concentrations in the western United States. *The Magazine for Environmental Managers* **June** (2019).
13. P. Yu, R. Xu, M. J. Abramson, S. Li, Y. Guo, Bushfires in Australia: a serious health emergency under climate change. *The Lancet Planetary Health* **4**, e7-e8 (2020).

14. S. Vardoulakis, B. B. Jalaludin, G. G. Morgan, I. C. Hanigan, F. H. Johnston, Bushfire smoke: urgent need for a national health protection strategy. *Medical Journal of Australia* **212**, 349 (2020).
15. A. van Donkelaar *et al.*, Satellite-based estimates of ground-level fine particulate matter during extreme events: A case study of the Moscow fires in 2010. *Atmospheric Environment* **45**, 6225-6232 (2011).
16. T. J. Yasunari *et al.*, Extreme air pollution events in Hokkaido, Japan, traced back to early snowmelt and large-scale wildfires over East Eurasia: Case studies. *Sci Rep* **8**, 6413 (2018).
17. P. Crippa *et al.*, Population exposure to hazardous air quality due to the 2015 fires in Equatorial Asia. *Sci Rep* **6**, 37074 (2016).
18. C. E. Reid *et al.*, Critical Review of Health Impacts of Wildfire Smoke Exposure. *Environ Health Perspect* **124**, 1334-1343 (2016).
19. K. O'Dell *et al.*, Hazardous Air Pollutants in Fresh and Aged Western US Wildfire Smoke and Implications for Long-Term Exposure. *Environmental Science & Technology* **54**, 11838-11847 (2020).
20. N. Borchers Arriagada *et al.*, Unprecedented smoke-related health burden associated with the 2019–20 bushfires in eastern Australia. *Medical Journal of Australia* **213**, 282-283 (2020).
21. N. Fann *et al.*, The health impacts and economic value of wildland fire episodes in the U.S.: 2008–2012. *Science of The Total Environment* **610-611**, 802-809 (2018).
22. USEPA, Treatment of data influenced by exceptional events. <https://www.epa.gov/air-quality-analysis/final-2016-exceptional-events-rule-supporting-guidance-documents-updated-faqs> (2007).
23. B. Ford *et al.*, Future Fire Impacts on Smoke Concentrations, Visibility, and Health in the Contiguous United States. *GeoHealth* **2**, 229-247 (2018).
24. E. N. Stavros, J. T. Abatzoglou, D. McKenzie, N. K. Larkin, Regional projections of the likelihood of very large wildland fires under a changing climate in the contiguous Western United States. *Climatic Change* **126**, 455-468 (2014).
25. J. T. Abatzoglou, A. P. Williams, R. Barbero, Global Emergence of Anthropogenic Climate Change in Fire Weather Indices. *Geophysical Research Letters* **46**, 326-336 (2019).

26. X. Yue, L. J. Mickley, J. A. Logan, J. O. Kaplan, Ensemble projections of wildfire activity and carbonaceous aerosol concentrations over the western United States in the mid-21st century. *Atmospheric Environment* **77**, 767-780 (2013).
27. J. S. Littell, D. McKenzie, H. Y. Wan, S. A. Cushman, Climate Change and Future Wildfire in the Western United States: An Ecological Approach to Nonstationarity. *Earth's Future* **6**, 1097-1111 (2018).
28. M. J. E. van Marle *et al.*, Historic global biomass burning emissions for CMIP6 (BB4CMIP) based on merging satellite observations with proxies and fire models (1750–2015). *Geoscientific Model Development* **10**, 3329-3357 (2017).
29. L. Feng *et al.*, The generation of gridded emissions data for CMIP6. *Geoscientific Model Development* **13**, 461-482 (2020).
30. Y. F. Lam, J. S. Fu, S. Wu, L. J. Mickley, Impacts of future climate change and effects of biogenic emissions on surface ozone and particulate matter concentrations in the United States. *Atmospheric Chemistry and Physics* **11**, 4789-4806 (2011).
31. W. J. Collins *et al.*, AerChemMIP: quantifying the effects of chemistry and aerosols in CMIP6. *Geoscientific Model Development* **10**, 585-607 (2017).
32. J. C. Liu *et al.*, Particulate Air Pollution from Wildfires in the Western US under Climate Change. *Clim Change* **138**, 655-666 (2016).
33. M. Val Martin *et al.*, How emissions, climate, and land use change will impact mid-century air quality over the United States: a focus on effects at national parks. *Atmospheric Chemistry and Physics* **15**, 2805-2823 (2015).
34. D. V. Spracklen *et al.*, Wildfires drive interannual variability of organic carbon aerosol in the western U.S. in summer. *Geophysical Research Letters* **34** (2007).
35. J. E. Neumann *et al.*, Estimating PM2.5-related premature mortality and morbidity associated with future wildfire emissions in the western US. *Environmental Research Letters* **16**, 035019 (2021).
36. D. Mills *et al.*, Projecting Age-Stratified Risk of Exposure to Inland Flooding and Wildfire Smoke in the United States under Two Climate Scenarios. *Environmental Health Perspectives* **126**, 047007 (2018).
37. W. Knorr, L. Jiang, A. Arneth, Climate, CO<sub>2</sub> and human population impacts on global wildfire emissions. *Biogeosciences* **13**, 267-282 (2016).

38. S. Kloster, N. M. Mahowald, J. T. Randerson, P. J. Lawrence, The impacts of climate, land use, and demography on fires during the 21st century simulated by CLM-CN. *Biogeosciences* **9**, 509-525 (2012).
39. D. McKenzie, J. S. Littel, Climate change and the eco-hydrology of fire: Will area burned increase in a warming western USA? *Ecological Applications* **27**, 26-36 (2017).
40. F. Li *et al.*, Historical (1700–2012) global multi-model estimates of the fire emissions from the Fire Modeling Intercomparison Project (FireMIP). *Atmospheric Chemistry and Physics* **19**, 12545-12567 (2019).
41. S. Kloster, G. Lasslop, Historical and future fire occurrence (1850 to 2100) simulated in CMIP5 Earth System Models. *Global and Planetary Change* **150**, 58-69 (2017).
42. F. Li, D. M. Lawrence, Role of Fire in the Global Land Water Budget during the Twentieth Century due to Changing Ecosystems. *Journal of Climate* **30**, 1893-1908 (2017).
43. D. S. Ward, E. Shevliakova, S. Malyshev, S. Rabin, Trends and Variability of Global Fire Emissions Due To Historical Anthropogenic Activities. *Global Biogeochemical Cycles* **32**, 122-142 (2018).
44. Y. Yu *et al.*, Increased Risk of the 2019 Alaskan July Fires due to Anthropogenic Activity. *Bulletin of the American Meteorological Society* **102**, S1-S7 (2021).
45. F. Li, X. D. Zeng, S. Levis, A process-based fire parameterization of intermediate complexity in a Dynamic Global Vegetation Model. *Biogeosciences* **9**, 2761-2780 (2012).
46. F. Li, B. Bond-Lamberty, S. Levis, Quantifying the role of fire in the Earth system – Part 2: Impact on the net carbon balance of global terrestrial ecosystems for the 20th century. *Biogeosciences* **11**, 1345-1360 (2014).
47. S. S. Rabin *et al.*, A fire model with distinct crop, pasture, and non-agricultural burning: use of new data and a model-fitting algorithm for FINAL.1. *Geosci. Model Dev.* **11**, 815-842 (2018).
48. S. S. Rabin *et al.*, The Fire Modeling Intercomparison Project (FireMIP), phase 1: experimental and analytical protocols with detailed model descriptions. *Geoscientific Model Development* **10**, 1175-1197 (2017).
49. D. M. Lawrence *et al.*, The Community Land Model Version 5: Description of New Features, Benchmarking, and Impact of Forcing Uncertainty. *Journal of Advances in Modeling Earth Systems* **11**, 4245-4287 (2019).

50. C. Delire *et al.*, The global land carbon cycle simulated with ISBA - CTRIP: Improvements over the last decade. *Journal of Advances in Modeling Earth Systems* **12**, e2019MS001886 (2020).
51. F. Li, S. Levis, D. S. Ward, Quantifying the role of fire in the Earth system-Part 1: Improved global fire modeling in the Community Earth System Model (CESM1). *Biogeosciences* **10**, 2293-2314 (2013).
52. A. P. K. Tai, L. J. Mickley, D. J. Jacob, Correlations between fine particulate matter (PM<sub>2.5</sub>) and meteorological variables in the United States: Implications for the sensitivity of PM<sub>2.5</sub> to climate change. *Atmospheric Environment* **44**, 3976-3984 (2010).
53. D. A. Jaffe *et al.*, Wildfire and prescribed burning impacts on air quality in the United States. *J Air Waste Manag Assoc* **70**, 583-615 (2020).
54. J. Balch *et al.*, Switching on the Big Burn of 2017. *Fire* **1**, 17 (2018).
55. NICC, National Interagency Coordination Center Report on Wildland fires and acres. [https://www.nifc.gov/fireInfo/fireInfo\\_statistics.html](https://www.nifc.gov/fireInfo/fireInfo_statistics.html), last assessed Nov. 2019 (2019).
56. P. E. Higuera, J. T. Abatzoglou, Record-setting climate enabled the extraordinary 2020 fire season in the western United States. *Global Change Biology* **27**, 1-2 (2021).
57. G. Danabasoglu *et al.*, The Community Earth System Model Version 2 (CESM2). *Journal of Advances in Modeling Earth Systems* **12** (2020).
58. J. P. Dunne *et al.*, The GFDL Earth System Model Version 4.1 (GFDL-ESM 4.1): Overall Coupled Model Description and Simulation Characteristics. *Journal of Advances in Modeling Earth Systems* **12**, e2019MS002015 (2020).
59. R. S  ferian *et al.*, Evaluation of CNRM Earth System Model, CNRM-ESM2-1: Role of Earth System Processes in Present-Day and Future Climate. *Journal of Advances in Modeling Earth Systems* **11**, 4182-4227 (2019).
60. L. Giglio, L. Boschetti, D. P. Roy, M. L. Humber, C. O. Justice, The Collection 6 MODIS burned area mapping algorithm and product. *Remote Sensing of Environment* **217**, 72-85 <ftp://ba71.geog.umd.edu> (2018).
61. J. T. Randerson, Y. Chen, G. R. Werf, B. M. Rogers, D. C. Morton, Global burned area and biomass burning emissions from small fires. *Journal of Geophysical Research: Biogeosciences* **117** (2012).
62. G. R. van der Werf *et al.*, Global fire emissions estimates during 1997–2016. *Earth System Science Data* **9**, 697-720 <https://www.globalfiredata.org/data.html> (2017).



63. A. Darmenov, A. M. da Silva, The Quick Fire Emissions Dataset (QFED)—Documentation of Versions 2.1, 2.2 and 2.4.  
<http://ftp.as.harvard.edu/gcgrid/data/ExtData/HEMCO/QFED/v2018-07/> (2015).
64. M. Hoerling *et al.*, Causes and Predictability of the 2012 Great Plains Drought. *Bulletin of the American Meteorological Society* **95**, 269-282 (2014).
65. F. Kogan, W. Guo, 2006–2015 mega-drought in the western USA and its monitoring from space data. *Geomatics, Natural Hazards and Risk* **6**, 651-668 (2015).
66. A. Hoell *et al.*, Anthropogenic Contributions to the Intensity of the 2017 United States Northern Great Plains Drought. *Bulletin of the American Meteorological Society* **100**, S19-S24 (2019).
67. D. LeComte, U.S. Weather Highlights 2018: Another Historic Hurricane and Wildfire Season. *Weatherwise* **72**, 12-23 (2019).
68. H. Wang, S. D. Schubert, R. D. Koster, Y. Chang, Attribution of the 2017 Northern High Plains Drought. *Bulletin of the American Meteorological Society* **100**, S25-S29 (2019).
69. M. Lin, L. W. Horowitz, R. Payton, A. M. Fiore, G. Tonnesen, US surface ozone trends and extremes from 1980 to 2014: quantifying the roles of rising Asian emissions, domestic controls, wildfires, and climate. *Atmospheric Chemistry and Physics* **17**, 2943-2970 (2017).
70. T. T. van Leeuwen *et al.*, Biomass burning fuel consumption rates: a field measurement database. *Biogeosciences* **11**, 7305-7329 (2014).
71. B. C. O'Neill *et al.*, The Scenario Model Intercomparison Project (ScenarioMIP) for CMIP6. *Geoscientific Model Development* **9**, 3461-3482 (2016).
72. K. Riahi *et al.*, The Shared Socioeconomic Pathways and their energy, land use, and greenhouse gas emissions implications: An overview. *Global Environmental Change* **42**, 153-168 (2017).
73. W. M. Jolly *et al.*, Climate-induced variations in global wildfire danger from 1979 to 2013. *Nat Commun* **6**, 7537 (2015).
74. K. L. Riley, R. A. Loehman, Mid-21st-century climate changes increase predicted fire occurrence and fire season length, Northern Rocky Mountains, United States. *Ecosphere* **7**, e01543 (2016).
75. E. K. Brown, J. Wang, Y. Feng, US wildfire potential: a historical view and future projection using high-resolution climate data. *Environmental Research Letters* **16** (2021).

76. L. M. Rasmijn *et al.*, Future equivalent of 2010 Russian heatwave intensified by weakening soil moisture constraints. *Nature Climate Change* **8**, 381-385 (2018).
77. L. Samaniego *et al.*, Anthropogenic warming exacerbates European soil moisture droughts. *Nature Climate Change* **8**, 421-426 (2018).
78. M. Lin *et al.*, Vegetation feedbacks during drought exacerbate ozone air pollution extremes in Europe. *Nature Climate Change* **10**, 444-451 (2020).
79. B. I. Cook *et al.*, Twenty - First Century Drought Projections in the CMIP6 Forcing Scenarios. *Earth's Future* **8** (2020).
80. J. S. Mankin, R. Seager, J. E. Smerdon, B. I. Cook, A. P. Williams, Mid-latitude freshwater availability reduced by projected vegetation responses to climate change. *Nature Geoscience* **12**, 983-988 (2019).
81. R. A. Fisher *et al.*, Parametric Controls on Vegetation Responses to Biogeochemical Forcing in the CLM5. *Journal of Advances in Modeling Earth Systems* **11**, 2879-2895 (2019).
82. S. Sitch *et al.*, Evaluation of the terrestrial carbon cycle, future plant geography and climate-carbon cycle feedbacks using five Dynamic Global Vegetation Models (DGVMs). *Global Change Biology* **14**, 2015-2039 (2008).
83. Z. Zhu *et al.*, Greening of the Earth and its drivers. *Nature Climate Change* **6**, 791-795 (2016).
84. K. C. Samir, W. Lutz, The human core of the shared socioeconomic pathways: Population scenarios by age, sex and level of education for all countries to 2100. *Global Environmental Change* **42**, 181-192 (2017).
85. N. Andela *et al.*, A human-driven decline in global burned area. *Science* **356**, 1356-1362 (2017).
86. F. Li, D. M. Lawrence, B. Bond-Lamberty, Human impacts on 20th century fire dynamics and implications for global carbon and water trajectories. *Global and Planetary Change* **162**, 18-27 (2018).
87. W. Knorr, A. Arneth, L. Jiang, Demographic controls of future global fire risk. *Nature Climate Change* **6**, 781-785 (2016).
88. F. Li, D. M. Lawrence, B. Bond-Lamberty, Impact of fire on global land surface air temperature and energy budget for the 20th century due to changes within ecosystems. *Environmental Research Letters* **12**, 044014 (2017).

89. G. Danabasoglu, NCAR CESM2 model output prepared for CMIP6 CMIP historical. Earth System Grid Federation. <https://doi.org/10.22033/ESGF/CMIP6.7627>.
90. J. P. Krasting *et al.*, NOAA-GFDL GFDL-ESM4 model output prepared for CMIP6 CMIP. Earth System Grid Federation. <https://doi.org/10.22033/ESGF/CMIP6.1407>.
91. R. Seferian, CNRM-CERFACS CNRM-ESM2-1 model output prepared for CMIP6 CMIP. Earth System Grid Federation. <https://doi.org/10.22033/ESGF/CMIP6.1391>.
92. L. M. Ulrike Groemping, Relative Importance of Regressors in Linear Models. <https://cran.r-project.org/web/packages/relaimpo/relaimpo.pdf> (2021).
93. M. Z. Al-Hamdan *et al.*, Methods for characterizing fine particulate matter using ground observations and remotely sensed data: potential use for environmental public health surveillance. *J Air Waste Manag Assoc* **59**, 865-881 (2009).
94. H. Hersbach *et al.*, The ERA5 global reanalysis. *Quarterly Journal of the Royal Meteorological Society* **146**, 1999-2049 (2020).
95. J. X. Wang, J. K. Angell, Air stagnation climatology for the United States. *NOAA/Air Resource Laboratory ATLAS* **1**, <https://www.ncdc.noaa.gov/societal-impacts/air-stagnation/maps> (1999).
96. S. Malyshev, E. Shevliakova, R. J. Stouffer, S. W. Pacala, Contrasting Local versus Regional Effects of Land-Use-Change-Induced Heterogeneity on Historical Climate: Analysis with the GFDL Earth System Model. *Journal of Climate* **28**, 5448-5469 (2015).
97. E. Shevliakova *et al.*, Carbon cycling under 300 years of land use change: Importance of the secondary vegetation sink. *Global Biogeochemical Cycles* **23** (2009).
98. E. S. Weng *et al.*, Scaling from individual trees to forests in an Earth system modeling framework using a mathematically tractable model of height-structured competition. *Biogeosciences* **12**, 2655-2694 (2015).
99. K. Thonicke, S. Venevsky, S. Sitch, W. Cramer, The role of fire disturbance for global vegetation dynamics: coupling fire into a Dynamic Global Vegetation Model. *Global Ecology and Biogeography* **10**, 661-677 (2001).
100. G. P. Compo *et al.*, The Twentieth Century Reanalysis Project. *Quarterly Journal of the Royal Meteorological Society* **137**, 1-28 (2011).

101. D. M. Lawrence *et al.*, The Land Use Model Intercomparison Project (LUMIP) contribution to CMIP6: rationale and experimental design. *Geoscientific Model Development* **9**, 2973-2998 (2016).
102. V. Eyring *et al.*, Overview of the Coupled Model Intercomparison Project Phase 6 (CMIP6) experimental design and organization. *Geoscientific Model Development* **9**, 1937-1958 (2016).
103. T. Hajima *et al.*, Development of the MIROC-ES2L Earth system model and the evaluation of biogeochemical processes and feedbacks. *Geoscientific Model Development* **13**, 2197-2244 (2020).
104. L. W. Horowitz *et al.*, The GFDL Global Atmospheric Chemistry-Climate Model AM4.1: Model Description and Simulation Characteristics. *Journal of Advances in Modeling Earth Systems* **12**, e2019MS002032 (2020).
105. Ø. Seland *et al.*, Overview of the Norwegian Earth System Model (NorESM2) and key climate response of CMIP6 DECK, historical, and scenario simulations. *Geosci. Model Dev.* **13**, 6165-6200 (2020).
106. S. G. Coles, An Introduction to Statistical Modeling of Extreme Values. *Springer, New York* (2001).
107. H. E. Rieder, A. M. Fiore, L. W. Horowitz, V. Naik, Projecting policy-relevant metrics for high summertime ozone pollution events over the eastern United States due to climate and emission changes during the 21st century. *Journal of Geophysical Research: Atmospheres* **120**, 784-800 (2015).
108. H. E. Rieder, A. M. Fiore, L. M. Polvani, J. F. Lamarque, Y. Fang, Changes in the frequency and return level of high ozone pollution events over the eastern United States following emission controls. *Environmental Research Letters* **8**, 014012 (2013).
109. L. Shen, L. J. Mickley, E. Gilleland, Impact of increasing heat waves on U.S. ozone episodes in the 2050s: Results from a multimodel analysis using extreme value theory. *Geophys Res Lett* **43**, 4017-4025 (2016).
110. E. Gilleland, R. W. Katz, extRemes2.0: An Extreme Value Analysis Package in R. *Journal of Statistical Software* **72** (2016).



## **Supplementary Information for**

### **Tripling of Western US Particulate Pollution from Wildfires in a Warming Climate**

Yuanyu Xie<sup>1,2\*</sup>, Meiyun Lin<sup>1,2\*</sup>, Bertrand Decharme<sup>3</sup>, Christine Delire<sup>3</sup>, Larry W. Horowitz<sup>2</sup>, David M. Lawrence<sup>4</sup>, Fang Li<sup>5</sup>, Roland Séférian<sup>3</sup>

**Corresponding authors:** Yuanyu Xie (Email: [Yuanyu.Xie@noaa.gov](mailto:Yuanyu.Xie@noaa.gov))

Meiyun Lin (Email: [Meiyun.Lin@noaa.gov](mailto:Meiyun.Lin@noaa.gov))

#### **This PDF file includes:**

- Texts S1 to S3
- Figures S1 to S14
- Tables S1 to S2
- SI References

## Supplementary Information Text

### Appendix S1. Cross validation of the MLR model

For each grid  $d$  with  $n$  years of available observations, we train the model using  $n-1$  years of data and predict over the remaining year. The resulting leave-one-out cross validation results for both the mean  $PM_{2.5}$  ( $r^2=0.56-0.61$ , root mean square error, RMSE =4.0–5.6  $\mu\text{g}/\text{m}^3$ ) and the 95th percentile  $PM_{2.5}$  ( $r^2=0.51-0.66$ , RMSE=11.3–14.1  $\mu\text{g}/\text{m}^3$ ) in August–September averaged over western US grids are statistically significant ( $p<0.05$ ). The results are close to the standard model fit ( $r^2=0.76-0.82$ , RMSE=2.3–7.7  $\mu\text{g}/\text{m}^3$ ), indicating robustness of the MLR model.

### Appendix S2. Meteorological dataset

Monthly mean surface temperature, precipitation and relative humidity are obtained from the European Centre for Medium-Range Weather Forecasts Reanalysis version 5 (ERA5) (94). The relative humidity is calculated from the dew point temperature in ERA5 as

$$RH = 100\% \times \frac{e_s(T_d)}{e_s(T)},$$

where  $T_d$  is the dewpoint temperature and  $T$  is the temperature, and  $e_s$  is the saturation vapor pressure, which can be empirically calculated using Bolton's method (111) in the form of

$$e_s(T) = 0.6112 \exp\left(\frac{17.67T}{T+243.5}\right),$$

Air stagnation in the U.S. National Centers for Environmental Information dataset is defined as days when there is no precipitation, sea level geostrophic winds are lower than 8 m/s (or <10 m/s when there is a surface to 850 mb temperature inversion), and 500 mb wind speeds are lower than 13 m/s (112). Air stagnation in the CMIP6 models is defined as days with precipitation smaller than 1 mm, surface wind speed lower than 3.2 m/s and 500 mb wind speeds lower than 13 m/s (113).

### Appendix S3. Fire modules in the three CMIP6 models

The fire module in CESM2 includes four components: non-peat fires outside croplands and tropical closed forests, agricultural fires in croplands, deforestation and degradation fires in the tropical closed forests, and peat fires (42, 45, 51). The burned area fraction is determined by climate and weather conditions, vegetation composition and structure, and human activities. Among them, human influence is represented by anthropogenic ignitions (increase with population density), fire suppression (increase with population density and gross domestic product per capita human), agricultural waste burning, and deforestation rate. After the calculation of burned area fraction, fire impacts are estimated, including fire emissions due to biomass and peat burning as well as plant-tissue mortality, which lead to adjustment of terrestrial ecosystem structure and functioning. We use the coupled simulations from CESM2-WACCM, a version of CESM2 with the same land model but with comprehensive chemistry extending to 130 km vertically (57, 114).

The fire module in GFDL-ESM4.1 is developed within a global dynamic vegetation and land surface model that comprises two sub-models for simulating agricultural and non-agricultural fires (43, 47, 97). The area burned for agricultural fires on cropland and pasture at each grid cell is forced with satellite observations of fire seasonality and frequency, depending on grid-scale crop and pasture area but not environmental changes. Simulation of non-agricultural fires follows the process-based fire model in CESM2, which predicts area burned at each grid cell as a product of the number of fires and burned area per fire, depending on grid-scale fuel availability, fuel moisture, and ignition source. Human fire suppression is represented as a function of population density. An enhanced fire rate of spread is introduced to better represent crown fires with high intensity. Non-agricultural fires are simulated on a daily basis, allowing multiday burning with a maximum duration of 30 days.  $\text{CO}_2$

emissions from fires are estimated by applying combustion completeness factors for different vegetation types on the aboveground biomass within the burned area.

CNRM-ESM2-1 represents natural wildfires over forests and grasslands in a land model that uses prescribed land use and land cover change files (50, 99). The grid cell fire fraction calculation was adapted to a daily timestep and depends on availability of fuel and fuel moisture, approximated by soil moisture and temperature. Fire fraction is set to zero when the surface litter carbon content is below 200 gC/m<sup>2</sup> and when soil temperature is lower than 0°C. It is also set to zero when more than 20% of the grid cell is covered by croplands. Except for this limitation on cropland, human fire suppression is not represented. Fire-induced emissions and fire effects on living and dead biomass are Plant Functional Type-dependent.

Supplementary Figures S1 to S14:

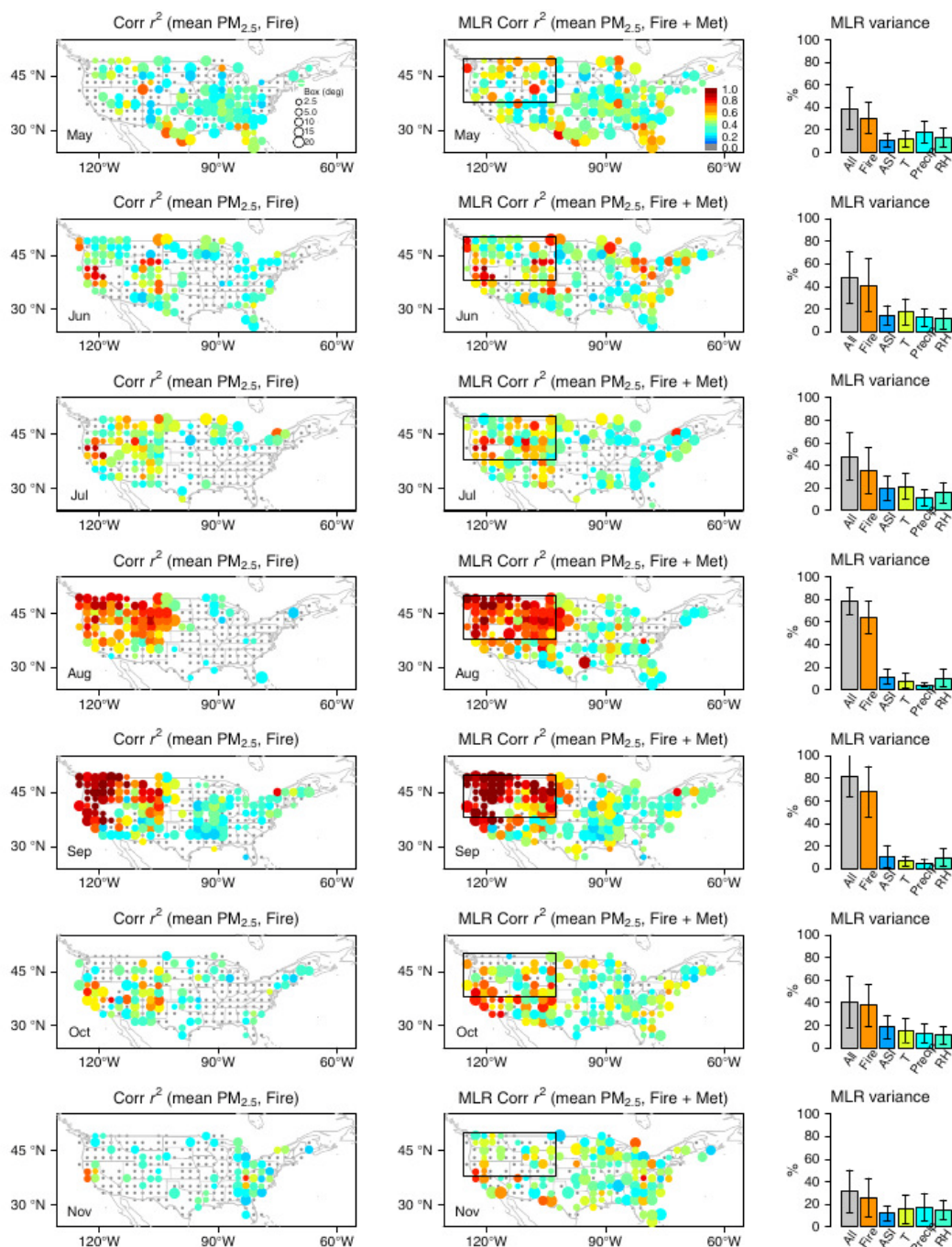


**Figure S1.** Observed correlations between fires and surface  $PM_{2.5}$  air quality. Correlation  $r^2$  of mean  $PM_{2.5}$  averaged over each  $2^\circ \times 2^\circ$  grid with regional total  $CO_2$  emissions from fires in May–November during 1997–2020, derived from simple linear regression (left panels) and multiple linear regression (middle panels) with consideration of meteorological variables, and the variance explained over the western US (black box on maps) by each predicting variable (right panels). The  $r^2$  values are color-coded for sites with significant correlations, with gray indicating sites with insignificant correlations ( $p$



> 0.05). The width of the box (in degrees), within which regional total fire emissions are best correlated with  $PM_{2.5}$  at that site, is given in the right corner in the top panel.

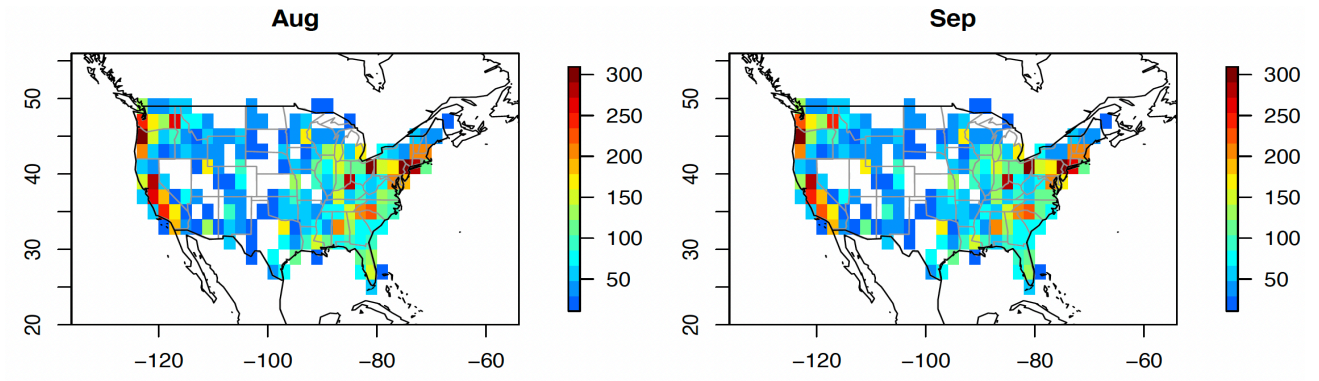
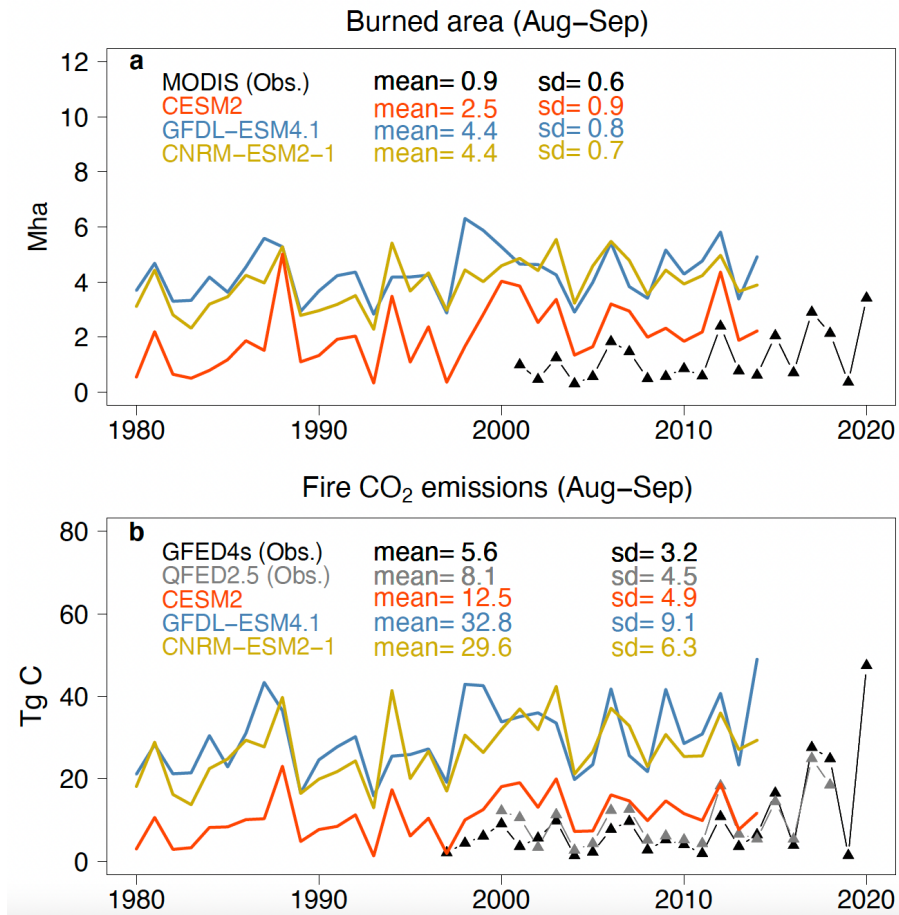
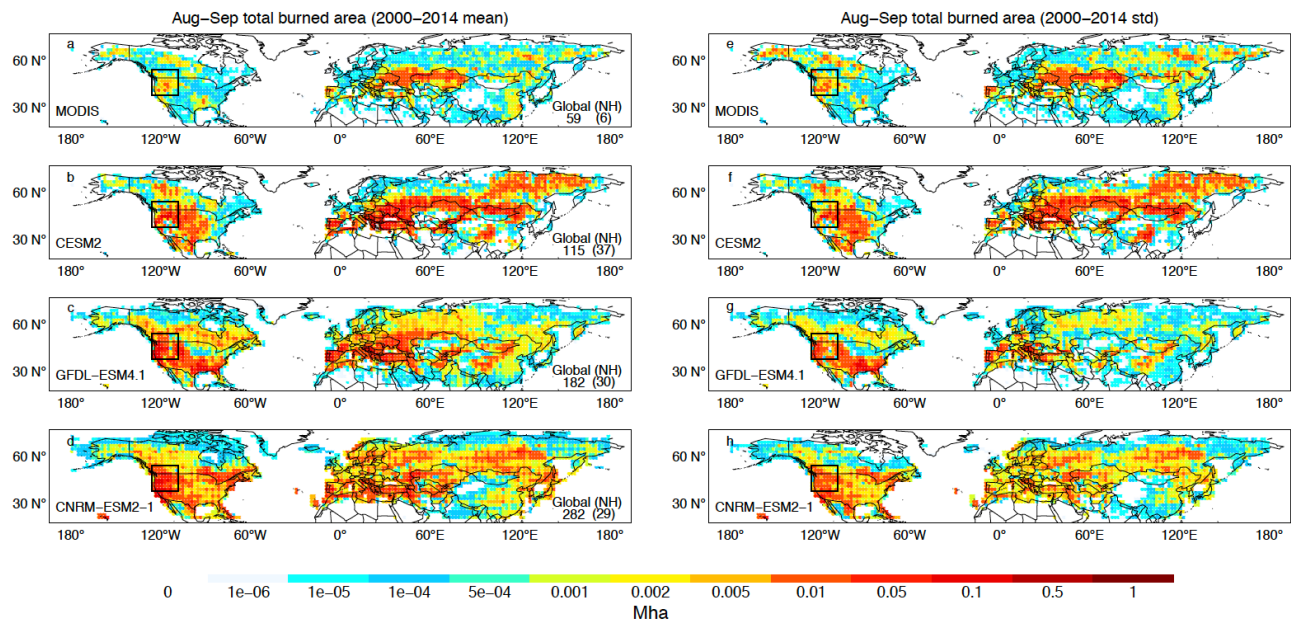


**Figure S2.** Sample sizes of surface PM<sub>2.5</sub> observations. Number of samples for calculating monthly means and q95 PM<sub>2.5</sub> at each 2°×2° grid in August and September averaged over 1997–2020.



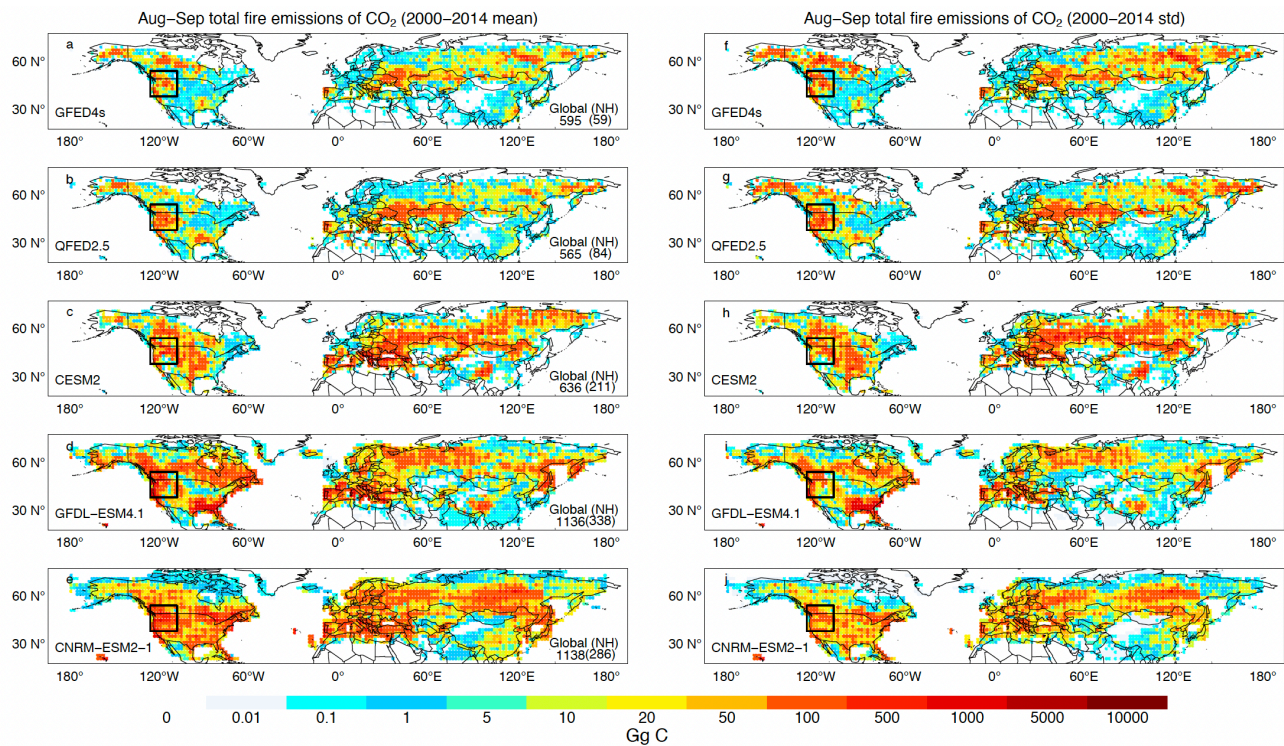
1

2 **Figure S3.** Evaluating model simulations of fires over western North America. (a) The August–September  
 3 total burned area over western North America (black box in Fig. S4) from 1980 to 2020 from MODIS satellite  
 4 observations (black) and from three CMIP6 land-only experiments (solid lines). (b) same as (a) but for fire  
 5 CO<sub>2</sub> emissions from two satellite observation-based inventories (black for GFED4s; gray for QFED2.5) and  
 6 from three CMIP6 land-only experiments (solid lines). Means and standard deviations (sd) during 2000–2014  
 7 are reported.



8

9 **Figure S4.** Spatial distribution of burned area from observations and land-only simulations. Mean (left panels)  
 10 and standard deviation (right panels) of the August–September total burned area during 2000–2014 from  
 11 MODIS satellite observations and from three CMIP6 land-only simulations. Black box represents western  
 12 North America where fire CO<sub>2</sub> emissions are integrated for analysis in Figs. 2-4. Global and Northern  
 13 Hemisphere total burned area (Mha) are reported at the right corner.



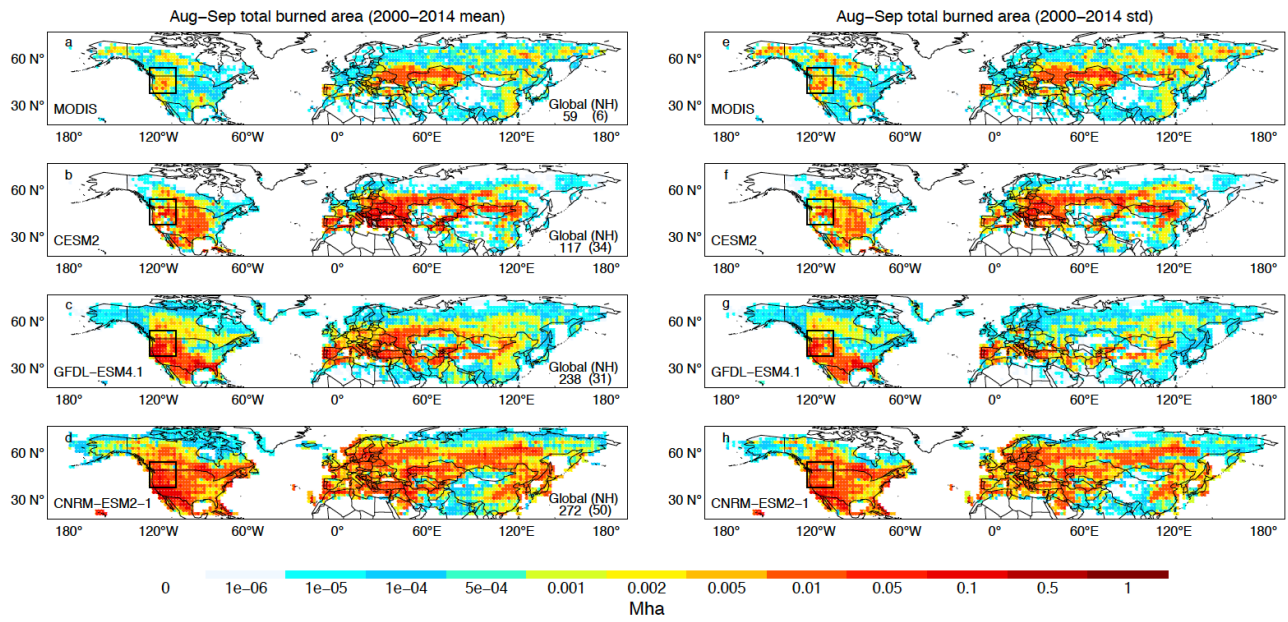
14

15 **Figure S5.** Spatial distribution of fire emissions of CO<sub>2</sub> from observations and land-only simulations. Mean  
 16 (left panels) and standard deviation (right panels) of the August–September total CO<sub>2</sub> emission from fires  
 17 during 2000–2014 from two satellite observation-based emission inventories (GFED4s and QFED2.5) and  
 18 from land-only experiments of three CMIP6 fire models driven by observation-based meteorological forcings.  
 19 Black box represents western North America where fire CO<sub>2</sub> emissions are integrated for analysis in Figs. 2–4.  
 20 Global and Northern Hemisphere total fire CO<sub>2</sub> emissions from fires (TgC) are reported at the right corner.

21

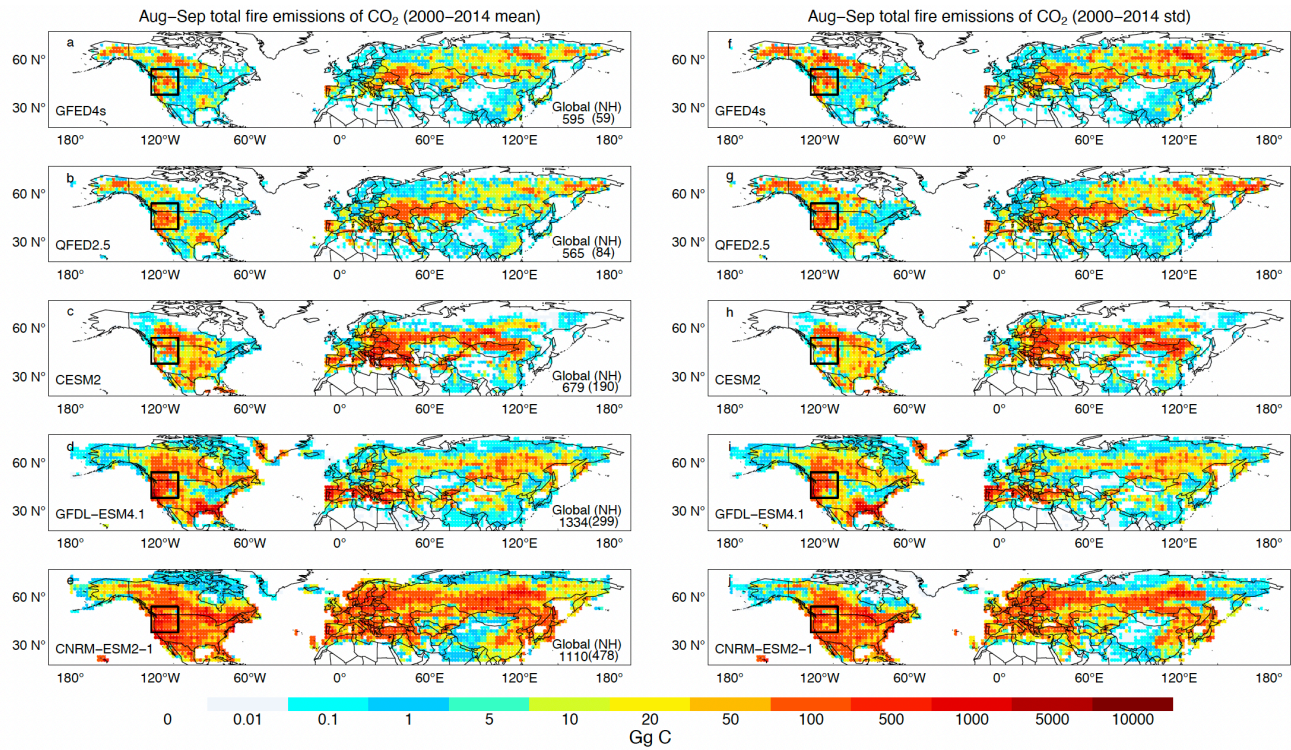
22

23



24

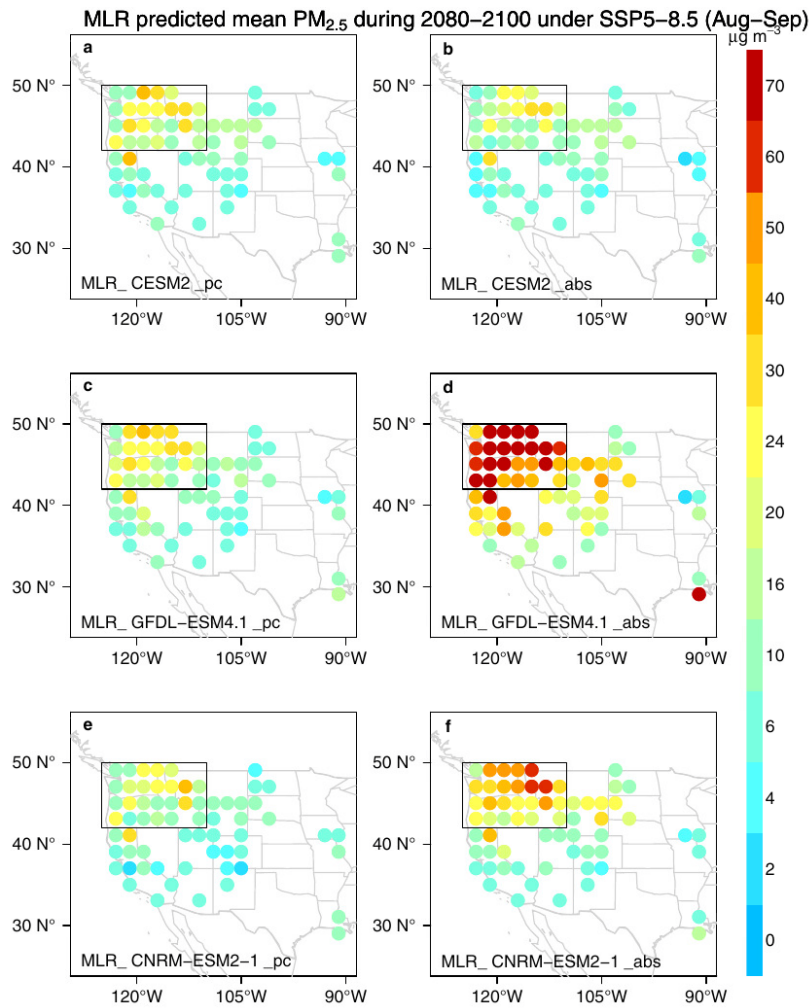
25 **Figure S6.** Same as Fig. S4, but with model results from the CMIP6 coupled model simulations.



26

27 **Figure S7.** Same as Fig. S5, but with model results from the CMIP6 coupled model simulations.

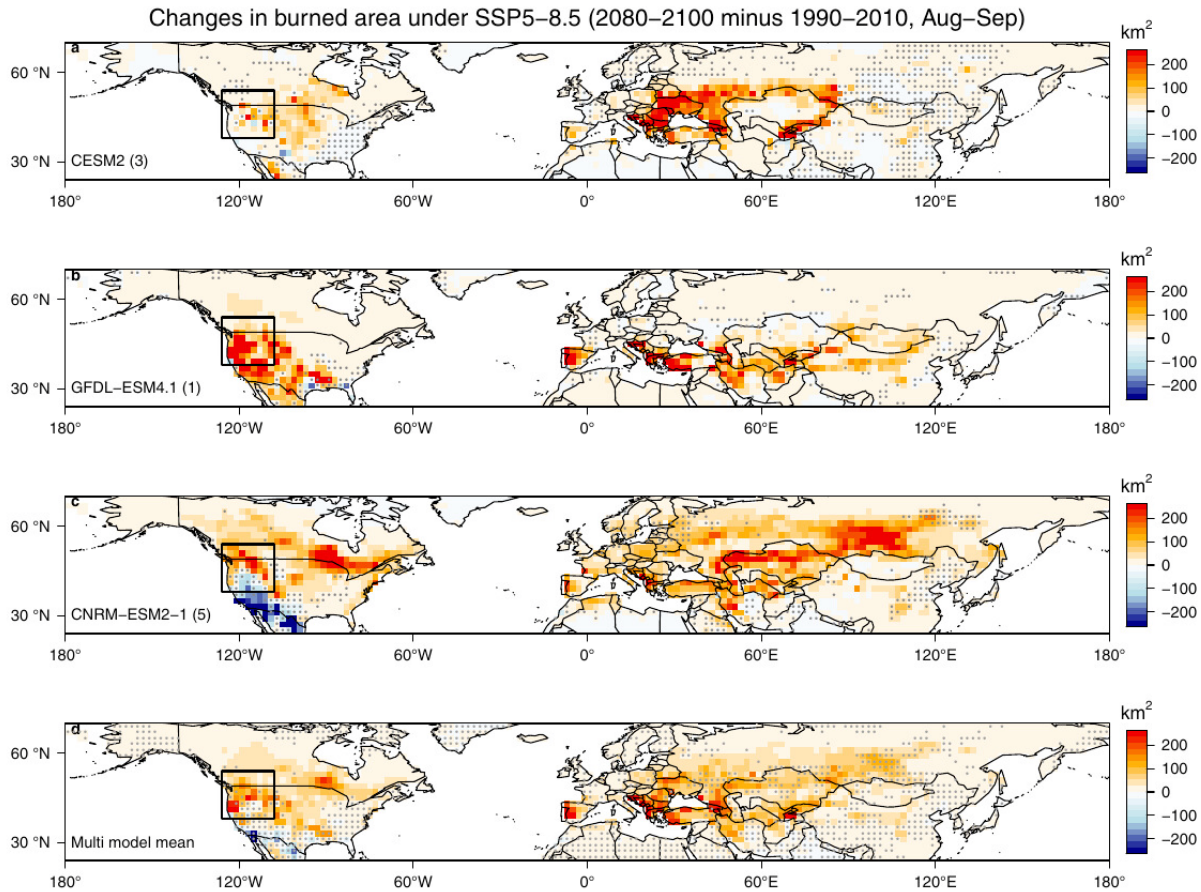
28



29

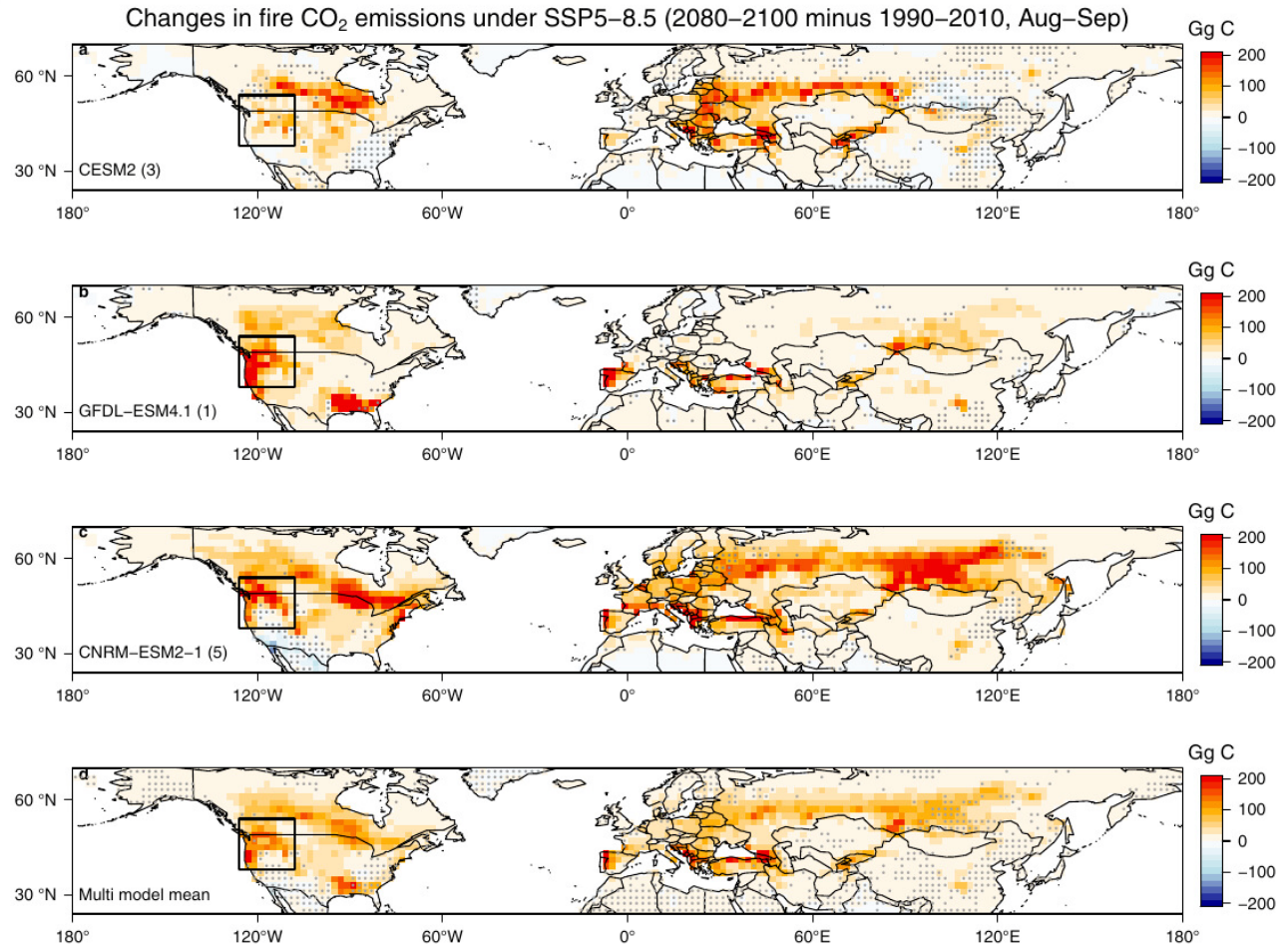
30 **Figure S8.** Uncertainties in MLR PM<sub>2.5</sub> predictions based on percentage versus absolute change of fires. (Left  
 31 panels) August–September mean PM<sub>2.5</sub> in the late 21<sup>st</sup> century (2080–2100) at western US sites (averaged  
 32 over a 2°×2° grid) predicted by MLR driven by the percentage change of fire CO<sub>2</sub> emissions under SSP5-8.5  
 33 relative to the respective 1990–2010 average from each CMIP6 fire model. (Right panels) same as the left  
 34 panels but driven by the absolute changes in each model. Only grids with MLR correlation  $r^2 > 0.5$  are shown.





36

37 **Figure S9.** Changes in burned area over northern mid-latitudes by three CMIP6 Earth system models.  
 38 Changes in the August–September total burned area during the late 21<sup>st</sup> century (2080–2100) compared to  
 39 present day (1990–2010) under SSP5-8.5 simulated by three CMIP6 models. Number of ensembles for each  
 40 model is shown in the parentheses at the bottom-left corner. The black box represents western North  
 41 America. Stippling indicates grids where the changes are not statistically significant at 95% confidence level  
 42 from >50% of the available ensembles. For multi model mean, the results are first averaged across the  
 43 available ensemble members from each model (3 for CESM2, 1 for GFDL-ESM4.1 and 5 for CNRM-ESM2-1),  
 44 and then averaged across the models. Stippling indicates grids with less than two models show statistically  
 45 significant ( $p < 0.05$ ) changes or the three models do not agree in sign. For each model, a change is defined  
 46 significant if >50% of the ensemble changes are statistically significant ( $p < 0.05$ ).



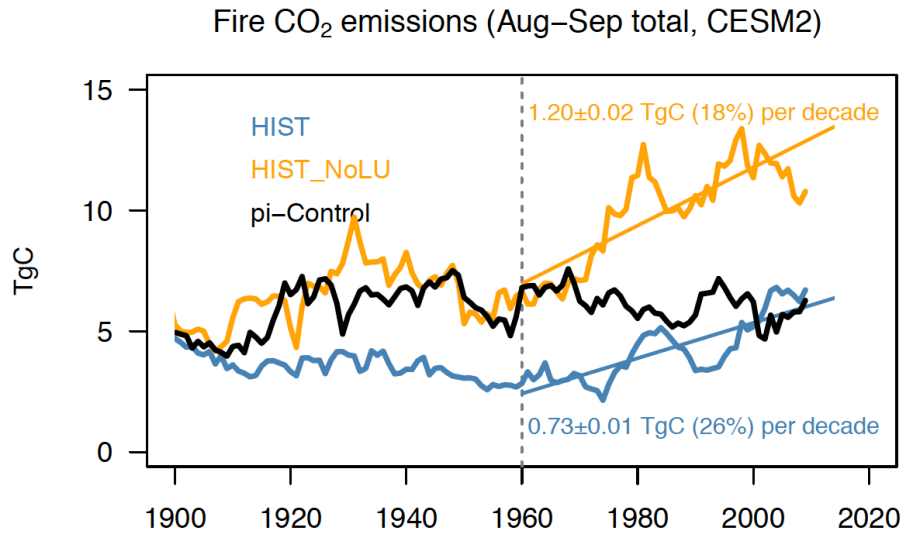
47

48 **Figure S10.** Same as Fig. S9, but for fire CO<sub>2</sub> emissions.

49

50

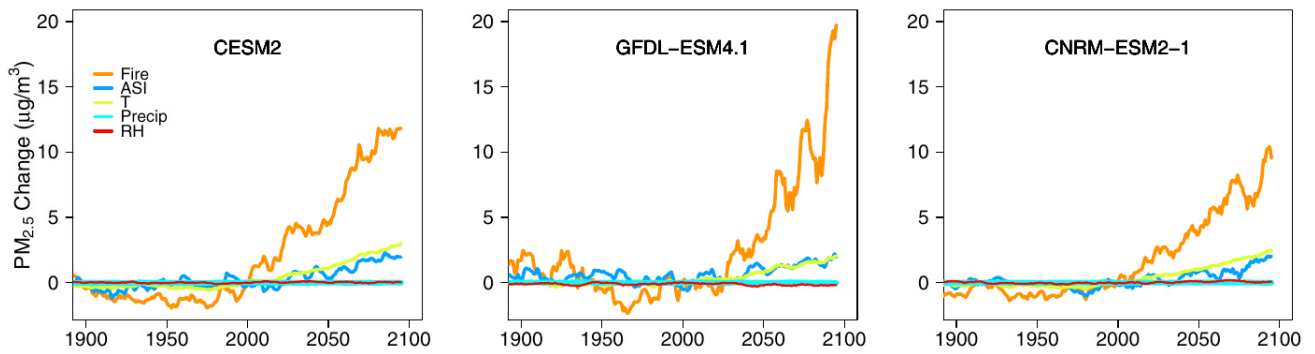
51



52

53 **Figure S11.** Historical evolution of fires over western North America. Temporal evolution of August–  
54 September total fire CO<sub>2</sub> emissions (10-year running average) over western North America during 1900–2014  
55 from CESM2 pre-industrial control simulation (pi-Control, black), coupled simulation with all forcings and  
56 historical land use and population density (HIST, blue), and coupled simulation with all forcings but with land  
57 use and population density held constant at 1850 level (HIST\_NoLU, orange). Linear trends (in absolute and  
58 percentage relative to 1960 level) during 1960–2014 as well as the 95% confidence limits are reported.

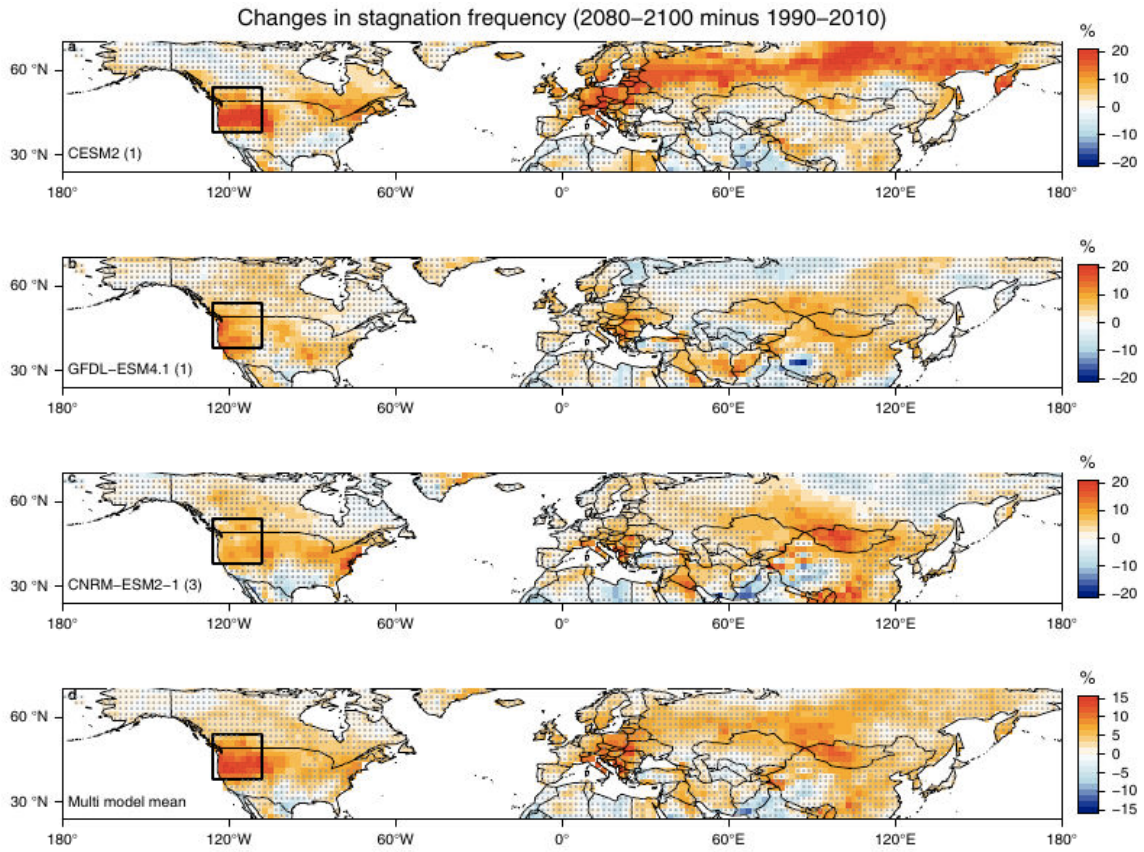
59



60

61 **Figure S12.** Projected changes in August–September mean  $PM_{2.5}$  from each predicting variable. The MLR  
 62 predicted 10-yr running average of changes in August–September mean  $PM_{2.5}$  averaged over the US Pacific  
 63 Northwest (black box in Fig. 5) based on the CMIP6 Earth system model projections of each predicting  
 64 variable: fire  $CO_2$  emissions (orange), air stagnation index (blue), surface temperature (green), precipitation  
 65 (cyan) and relative humidity (red).

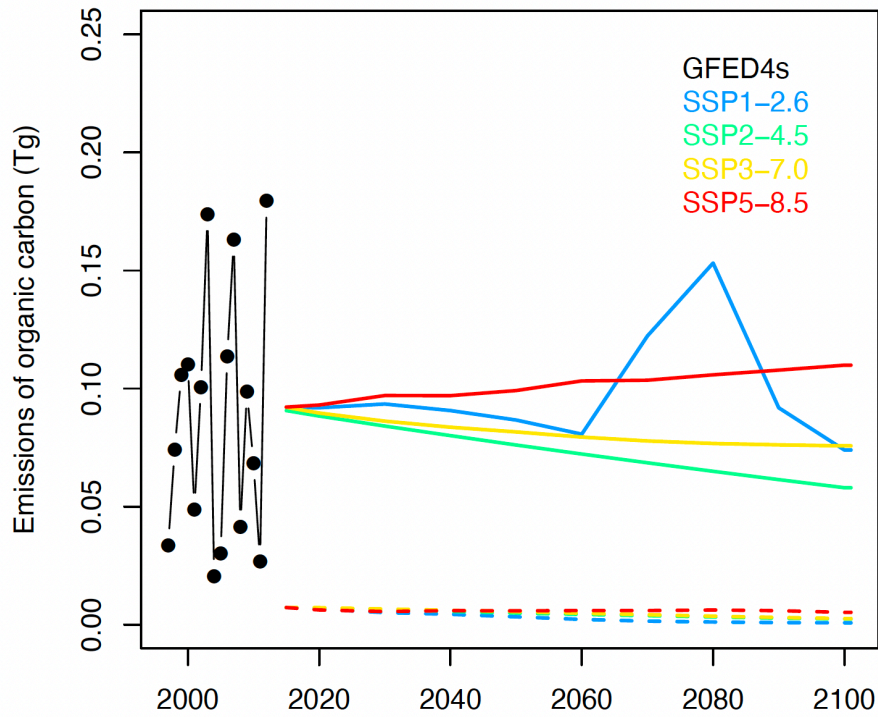
66



68 **Figure S13.** Same as Fig. S9, but for air stagnation frequency.

69

70



71

72 **Figure S14.** Prescribed organic carbon emissions used for chemistry-climate model PM<sub>2.5</sub>  
 73 predictions. Shown are August–September total organic carbon emissions over western North  
 74 America from biomass burning (color-coded solid lines) and anthropogenic sources (color-coded  
 75 dashed lines) during 2015–2100 under four SSPs. Prescribed fire emissions from GFED4s for  
 76 historical simulations (before 2014; black) are also shown.

77

78 **Supplementary Tables 1 and 2**

79 **Table S1** List of CMIP6 fire models, and number of ensembles from each experiment.

Models	Land-only	Coupled Historical	Coupled SSP1-2.6	Coupled SSP2-4.5	Coupled SSP3-7.0	Coupled SSP5-8.5
	1850–2014		2015–2100			
CESM2 (1.25°×0.94°)	1	3	1	3	3	3
GFDL-ESM4.1 (1.25°×1°)	1	3	1	3	1	1
CNRM-ESM2-1 (1.4°×1.4°)	1	5	5	5	5	5

80

81 **Table S2** Multi-ensemble means of changes in fire CO<sub>2</sub> emissions (in percent relative to 1990–2010)  
 82 over western North America and the MLR-predicted PM<sub>2.5</sub> (µg/m<sup>3</sup>; percentage changes in  
 83 parenthesis) averaged over US Pacific Northwest sites by late 21<sup>st</sup> century (2080–2100).

Models	SSP1-2.6	SSP2-4.5	SSP3-7.0	SSP5-8.5
	Fire CO <sub>2</sub> emissions, August–September			
CESM2	+113%	+145%	+254%	+242%
GFDL-ESM4.1	+70%	+121%	+202%	+262%
CNRM-ESM2-1	+60%	+100%	+110%	+133%
	Mean PM <sub>2.5</sub> (US Pacific Northwest), August–September			
MLR (CESM2)	15.4 (+62%)	18.4 (+93%)	22.7 (+138%)	23.9 (+150%)
MLR (GFDL-ESM4.1)	12.7 (+34%)	17.8 (+87%)	22.4 (+135%)	24.8 (+160%)
MLR (CNRM-ESM2-1)	13.2 (+39%)	16.6 (+74%)	18.9 (+99%)	18.9 (+99%)
	q95 PM <sub>2.5</sub> (US Pacific Northwest), August–September			
MLR (CESM2)	46.4 (+91%)	55.8 (+129%)	73.0 (+201%)	76.9 (+217%)
MLR (GFDL-ESM4.1)	39.1 (+61%)	57.2 (+136%)	73.6 (+203%)	81.6 (+236%)
MLR (CNRM-ESM2-1)	38.1 (+57%)	50.4 (+108%)	56.4 (+132%)	58.0 (+139%)

84



85

86

87

88 **SI References**

89

- 90 1. USEPA, Data from the 2017 National Emissions Inventory. [https://www.epa.gov/air-](https://www.epa.gov/air-emissions-inventories/2017-national-emissions-inventory-nei-data)  
91 [emissions-inventories/2017-national-emissions-inventory-nei-data](https://www.epa.gov/air-emissions-inventories/2017-national-emissions-inventory-nei-data) (2017).
- 92 2. D. M. J. S. Bowman *et al.*, Vegetation fires in the Anthropocene. *Nature Reviews Earth &*  
93 *Environment* **1**, 500-515 (2020).
- 94 3. F. H. Johnston *et al.*, Estimated Global Mortality Attributable to Smoke from Landscape Fires.  
95 *Environmental Health Perspectives* **120**, 695-701 (2012).
- 96 4. M. Burke *et al.*, The changing risk and burden of wildfire in the United States. *Proceedings of*  
97 *the National Academy of Sciences* **118**, e2011048118 (2021).
- 98 5. G. P. Schill *et al.*, Widespread biomass burning smoke throughout the remote troposphere.  
99 *Nature Geoscience* **13**, 422-427 (2020).
- 100 6. A. L. Westerling, H. G. Hidalgo, D. R. Cayan, T. W. Swetnam, Warming and earlier spring  
101 increase western US forest wildfire activity. *Science* **313**, 940-943 (2006).
- 102 7. A. L. Westerling, Increasing western US forest wildfire activity: sensitivity to changes in the  
103 timing of spring. *Philos Trans R Soc Lond B Biol Sci* **371** (2016).
- 104 8. J. T. Abatzoglou, A. P. Williams, Impact of anthropogenic climate change on wildfire across  
105 western US forests. *Proceedings of the National Academy of Sciences* **113**, 11770-11775  
106 (2016).
- 107 9. C. D. McClure, D. A. Jaffe, US particulate matter air quality improves except in wildfire-prone  
108 areas. *Proceedings of the National Academy of Sciences* **115**, 7901-7906 (2018).
- 109 10. K. O'Dell, B. Ford, E. V. Fischer, J. R. Pierce, Contribution of Wildland-Fire Smoke to US PM<sub>2.5</sub>  
110 and Its Influence on Recent Trends. *Environmental Science & Technology* **53**, 1797-1804  
111 (2019).
- 112 11. Y. Xie, M. Lin, L. W. Horowitz, Summer PM<sub>2.5</sub> pollution extremes caused by wildfires over  
113 the western United States during 2017–2018. *Geophysical Research Letters* **47**,  
114 e2020GL089429 (2020).

- 115 12. R. J. Laing, D. A. Jaffe, Wildfires are causing extreme PM concentrations in the western  
116 United States. *The Magazine for Environmental Managers* **June** (2019).
- 117 13. P. Yu, R. Xu, M. J. Abramson, S. Li, Y. Guo, Bushfires in Australia: a serious health emergency  
118 under climate change. *The Lancet Planetary Health* **4**, e7-e8 (2020).
- 119 14. S. Vardoulakis, B. B. Jalaludin, G. G. Morgan, I. C. Hanigan, F. H. Johnston, Bushfire smoke:  
120 urgent need for a national health protection strategy. *Medical Journal of Australia* **212**, 349  
121 (2020).
- 122 15. A. van Donkelaar *et al.*, Satellite-based estimates of ground-level fine particulate matter  
123 during extreme events: A case study of the Moscow fires in 2010. *Atmospheric Environment*  
124 **45**, 6225-6232 (2011).
- 125 16. T. J. Yasunari *et al.*, Extreme air pollution events in Hokkaido, Japan, traced back to early  
126 snowmelt and large-scale wildfires over East Eurasia: Case studies. *Sci Rep* **8**, 6413 (2018).
- 127 17. P. Crippa *et al.*, Population exposure to hazardous air quality due to the 2015 fires in  
128 Equatorial Asia. *Sci Rep* **6**, 37074 (2016).
- 129 18. C. E. Reid *et al.*, Critical Review of Health Impacts of Wildfire Smoke Exposure. *Environ Health*  
130 *Perspect* **124**, 1334-1343 (2016).
- 131 19. K. O'Dell *et al.*, Hazardous Air Pollutants in Fresh and Aged Western US Wildfire Smoke and  
132 Implications for Long-Term Exposure. *Environmental Science & Technology* **54**, 11838-11847  
133 (2020).
- 134 20. N. Borchers Arriagada *et al.*, Unprecedented smoke-related health burden associated with  
135 the 2019–20 bushfires in eastern Australia. *Medical Journal of Australia* **213**, 282-283 (2020).
- 136 21. N. Fann *et al.*, The health impacts and economic value of wildland fire episodes in the U.S.:  
137 2008–2012. *Science of The Total Environment* **610-611**, 802-809 (2018).
- 138 22. USEPA, Treatment of data influenced by exceptional events. [https://www.epa.gov/air-](https://www.epa.gov/air-quality-analysis/final-2016-exceptional-events-rule-supporting-guidance-documents-updated-faqs)  
139 [quality-analysis/final-2016-exceptional-events-rule-supporting-guidance-documents-](https://www.epa.gov/air-quality-analysis/final-2016-exceptional-events-rule-supporting-guidance-documents-updated-faqs)  
140 [updated-faqs](https://www.epa.gov/air-quality-analysis/final-2016-exceptional-events-rule-supporting-guidance-documents-updated-faqs) (2007).
- 141 23. B. Ford *et al.*, Future Fire Impacts on Smoke Concentrations, Visibility, and Health in the  
142 Contiguous United States. *GeoHealth* **2**, 229-247 (2018).
- 143 24. E. N. Stavros, J. T. Abatzoglou, D. McKenzie, N. K. Larkin, Regional projections of the  
144 likelihood of very large wildland fires under a changing climate in the contiguous Western  
145 United States. *Climatic Change* **126**, 455-468 (2014).

- 146 25. J. T. Abatzoglou, A. P. Williams, R. Barbero, Global Emergence of Anthropogenic Climate  
147 Change in Fire Weather Indices. *Geophysical Research Letters* **46**, 326-336 (2019).
- 148 26. X. Yue, L. J. Mickley, J. A. Logan, J. O. Kaplan, Ensemble projections of wildfire activity and  
149 carbonaceous aerosol concentrations over the western United States in the mid-21st  
150 century. *Atmospheric Environment* **77**, 767-780 (2013).
- 151 27. J. S. Littell, D. McKenzie, H. Y. Wan, S. A. Cushman, Climate Change and Future Wildfire in the  
152 Western United States: An Ecological Approach to Nonstationarity. *Earth's Future* **6**, 1097-  
153 1111 (2018).
- 154 28. M. J. E. van Marle *et al.*, Historic global biomass burning emissions for CMIP6 (BB4CMIP)  
155 based on merging satellite observations with proxies and fire models (1750–2015).  
156 *Geoscientific Model Development* **10**, 3329-3357 (2017).
- 157 29. L. Feng *et al.*, The generation of gridded emissions data for CMIP6. *Geoscientific Model*  
158 *Development* **13**, 461-482 (2020).
- 159 30. Y. F. Lam, J. S. Fu, S. Wu, L. J. Mickley, Impacts of future climate change and effects of  
160 biogenic emissions on surface ozone and particulate matter concentrations in the United  
161 States. *Atmospheric Chemistry and Physics* **11**, 4789-4806 (2011).
- 162 31. W. J. Collins *et al.*, AerChemMIP: quantifying the effects of chemistry and aerosols in CMIP6.  
163 *Geoscientific Model Development* **10**, 585-607 (2017).
- 164 32. J. C. Liu *et al.*, Particulate Air Pollution from Wildfires in the Western US under Climate  
165 Change. *Clim Change* **138**, 655-666 (2016).
- 166 33. M. Val Martin *et al.*, How emissions, climate, and land use change will impact mid-century air  
167 quality over the United States: a focus on effects at national parks. *Atmospheric Chemistry*  
168 *and Physics* **15**, 2805-2823 (2015).
- 169 34. D. V. Spracklen *et al.*, Wildfires drive interannual variability of organic carbon aerosol in the  
170 western U.S. in summer. *Geophysical Research Letters* **34** (2007).
- 171 35. J. E. Neumann *et al.*, Estimating PM2.5-related premature mortality and morbidity  
172 associated with future wildfire emissions in the western US. *Environmental Research Letters*  
173 **16**, 035019 (2021).
- 174 36. D. Mills *et al.*, Projecting Age-Stratified Risk of Exposure to Inland Flooding and Wildfire  
175 Smoke in the United States under Two Climate Scenarios. *Environmental Health Perspectives*  
176 **126**, 047007 (2018).

- 177 37. W. Knorr, L. Jiang, A. Arneth, Climate, CO<sub>2</sub> and human population impacts on global wildfire  
178 emissions. *Biogeosciences* **13**, 267-282 (2016).
- 179 38. S. Kloster, N. M. Mahowald, J. T. Randerson, P. J. Lawrence, The impacts of climate, land use,  
180 and demography on fires during the 21st century simulated by CLM-CN. *Biogeosciences* **9**,  
181 509-525 (2012).
- 182 39. D. McKenzie, J. S. Littell, Climate change and the eco-hydrology of fire: Will area burned  
183 increase in a warming western USA? *Ecological Applications* **27**, 26-36 (2017).
- 184 40. F. Li *et al.*, Historical (1700–2012) global multi-model estimates of the fire emissions from the  
185 Fire Modeling Intercomparison Project (FireMIP). *Atmospheric Chemistry and Physics* **19**,  
186 12545-12567 (2019).
- 187 41. S. Kloster, G. Lasslop, Historical and future fire occurrence (1850 to 2100) simulated in CMIP5  
188 Earth System Models. *Global and Planetary Change* **150**, 58-69 (2017).
- 189 42. F. Li, D. M. Lawrence, Role of Fire in the Global Land Water Budget during the Twentieth  
190 Century due to Changing Ecosystems. *Journal of Climate* **30**, 1893-1908 (2017).
- 191 43. D. S. Ward, E. Shevliakova, S. Malyshev, S. Rabin, Trends and Variability of Global Fire  
192 Emissions Due To Historical Anthropogenic Activities. *Global Biogeochemical Cycles* **32**, 122-  
193 142 (2018).
- 194 44. Y. Yu *et al.*, Increased Risk of the 2019 Alaskan July Fires due to Anthropogenic Activity.  
195 *Bulletin of the American Meteorological Society* **102**, S1-S7 (2021).
- 196 45. F. Li, X. D. Zeng, S. Levis, A process-based fire parameterization of intermediate complexity in  
197 a Dynamic Global Vegetation Model. *Biogeosciences* **9**, 2761-2780 (2012).
- 198 46. F. Li, B. Bond-Lamberty, S. Levis, Quantifying the role of fire in the Earth system – Part 2:  
199 Impact on the net carbon balance of global terrestrial ecosystems for the 20th century.  
200 *Biogeosciences* **11**, 1345-1360 (2014).
- 201 47. S. S. Rabin *et al.*, A fire model with distinct crop, pasture, and non-agricultural burning: use  
202 of new data and a model-fitting algorithm for FINAL.1. *Geosci. Model Dev.* **11**, 815-842  
203 (2018).
- 204 48. S. S. Rabin *et al.*, The Fire Modeling Intercomparison Project (FireMIP), phase 1: experimental  
205 and analytical protocols with detailed model descriptions. *Geoscientific Model Development*  
206 **10**, 1175-1197 (2017).

- 207 49. D. M. Lawrence *et al.*, The Community Land Model Version 5: Description of New Features,  
208 Benchmarking, and Impact of Forcing Uncertainty. *Journal of Advances in Modeling Earth*  
209 *Systems* **11**, 4245-4287 (2019).
- 210 50. C. Delire *et al.*, The global land carbon cycle simulated with ISBA-CTRIP: Improvements over  
211 the last decade. *Journal of Advances in Modeling Earth Systems* **12**, e2019MS001886 (2020).
- 212 51. F. Li, S. Levis, D. S. Ward, Quantifying the role of fire in the Earth system-Part 1: Improved  
213 global fire modeling in the Community Earth System Model (CESM1). *Biogeosciences* **10**,  
214 2293-2314 (2013).
- 215 52. A. P. K. Tai, L. J. Mickley, D. J. Jacob, Correlations between fine particulate matter (PM<sub>2.5</sub>) and  
216 meteorological variables in the United States: Implications for the sensitivity of PM<sub>2.5</sub> to  
217 climate change. *Atmospheric Environment* **44**, 3976-3984 (2010).
- 218 53. D. A. Jaffe *et al.*, Wildfire and prescribed burning impacts on air quality in the United States. *J*  
219 *Air Waste Manag Assoc* **70**, 583-615 (2020).
- 220 54. J. Balch *et al.*, Switching on the Big Burn of 2017. *Fire* **1**, 17 (2018).
- 221 55. NICC, National Interagency Coordination Center Report on Wildland fires and acres.  
222 [https://www.nifc.gov/fireInfo/fireInfo\\_statistics.html](https://www.nifc.gov/fireInfo/fireInfo_statistics.html), last assessed Nov. 2019 (2019).
- 223 56. P. E. Higuera, J. T. Abatzoglou, Record-setting climate enabled the extraordinary 2020 fire  
224 season in the western United States. *Global Change Biology* **27**, 1-2 (2021).
- 225 57. G. Danabasoglu *et al.*, The Community Earth System Model Version 2 (CESM2). *Journal of*  
226 *Advances in Modeling Earth Systems* **12** (2020).
- 227 58. J. P. Dunne *et al.*, The GFDL Earth System Model Version 4.1 (GFDL-ESM 4.1): Overall Coupled  
228 Model Description and Simulation Characteristics. *Journal of Advances in Modeling Earth*  
229 *Systems* **12**, e2019MS002015 (2020).
- 230 59. R. Séférian *et al.*, Evaluation of CNRM Earth System Model, CNRM-ESM2-1: Role of Earth  
231 System Processes in Present-Day and Future Climate. *Journal of Advances in Modeling Earth*  
232 *Systems* **11**, 4182-4227 (2019).
- 233 60. L. Giglio, L. Boschetti, D. P. Roy, M. L. Humber, C. O. Justice, The Collection 6 MODIS burned  
234 area mapping algorithm and product. *Remote Sensing of Environment* **217**, 72-85  
235 <ftp://ba71.geog.umd.edu> (2018).

- 236 61. J. T. Randerson, Y. Chen, G. R. Werf, B. M. Rogers, D. C. Morton, Global burned area and  
237 biomass burning emissions from small fires. *Journal of Geophysical Research: Biogeosciences*  
238 **117** (2012).
- 239 62. G. R. van der Werf *et al.*, Global fire emissions estimates during 1997–2016. *Earth System*  
240 *Science Data* **9**, 697-720 <https://www.globalfiredata.org/data.html> (2017).
- 241 63. A. Darmenov, A. M. da Silva, The Quick Fire Emissions Dataset (QFED)—Documentation of  
242 Versions 2.1, 2.2 and 2.4.  
243 <http://ftp.as.harvard.edu/gcgrid/data/ExtData/HEMCO/QFED/v2018-07/> (2015).
- 244 64. M. Hoerling *et al.*, Causes and Predictability of the 2012 Great Plains Drought. *Bulletin of the*  
245 *American Meteorological Society* **95**, 269-282 (2014).
- 246 65. F. Kogan, W. Guo, 2006–2015 mega-drought in the western USA and its monitoring from  
247 space data. *Geomatics, Natural Hazards and Risk* **6**, 651-668 (2015).
- 248 66. A. Hoell *et al.*, Anthropogenic Contributions to the Intensity of the 2017 United States  
249 Northern Great Plains Drought. *Bulletin of the American Meteorological Society* **100**, S19-S24  
250 (2019).
- 251 67. D. LeComte, U.S. Weather Highlights 2018: Another Historic Hurricane and Wildfire Season.  
252 *Weatherwise* **72**, 12-23 (2019).
- 253 68. H. Wang, S. D. Schubert, R. D. Koster, Y. Chang, Attribution of the 2017 Northern High Plains  
254 Drought. *Bulletin of the American Meteorological Society* **100**, S25-S29 (2019).
- 255 69. M. Lin, L. W. Horowitz, R. Payton, A. M. Fiore, G. Tonnesen, US surface ozone trends and  
256 extremes from 1980 to 2014: quantifying the roles of rising Asian emissions, domestic  
257 controls, wildfires, and climate. *Atmospheric Chemistry and Physics* **17**, 2943-2970 (2017).
- 258 70. T. T. van Leeuwen *et al.*, Biomass burning fuel consumption rates: a field measurement  
259 database. *Biogeosciences* **11**, 7305-7329 (2014).
- 260 71. B. C. O'Neill *et al.*, The Scenario Model Intercomparison Project (ScenarioMIP) for CMIP6.  
261 *Geoscientific Model Development* **9**, 3461-3482 (2016).
- 262 72. K. Riahi *et al.*, The Shared Socioeconomic Pathways and their energy, land use, and  
263 greenhouse gas emissions implications: An overview. *Global Environmental Change* **42**, 153-  
264 168 (2017).
- 265 73. W. M. Jolly *et al.*, Climate-induced variations in global wildfire danger from 1979 to 2013. *Nat*  
266 *Commun* **6**, 7537 (2015).

- 267 74. K. L. Riley, R. A. Loehman, Mid-21st-century climate changes increase predicted fire  
268 occurrence and fire season length, Northern Rocky Mountains, United States. *Ecosphere* **7**,  
269 e01543 (2016).
- 270 75. E. K. Brown, J. Wang, Y. Feng, US wildfire potential: a historical view and future projection  
271 using high-resolution climate data. *Environmental Research Letters* **16** (2021).
- 272 76. L. M. Rasmijn *et al.*, Future equivalent of 2010 Russian heatwave intensified by weakening  
273 soil moisture constraints. *Nature Climate Change* **8**, 381-385 (2018).
- 274 77. L. Samaniego *et al.*, Anthropogenic warming exacerbates European soil moisture droughts.  
275 *Nature Climate Change* **8**, 421-426 (2018).
- 276 78. M. Lin *et al.*, Vegetation feedbacks during drought exacerbate ozone air pollution extremes in  
277 Europe. *Nature Climate Change* **10**, 444-451 (2020).
- 278 79. B. I. Cook *et al.*, Twenty-First Century Drought Projections in the CMIP6 Forcing Scenarios.  
279 *Earth's Future* **8** (2020).
- 280 80. J. S. Mankin, R. Seager, J. E. Smerdon, B. I. Cook, A. P. Williams, Mid-latitude freshwater  
281 availability reduced by projected vegetation responses to climate change. *Nature Geoscience*  
282 **12**, 983-988 (2019).
- 283 81. R. A. Fisher *et al.*, Parametric Controls on Vegetation Responses to Biogeochemical Forcing in  
284 the CLM5. *Journal of Advances in Modeling Earth Systems* **11**, 2879-2895 (2019).
- 285 82. S. Sitch *et al.*, Evaluation of the terrestrial carbon cycle, future plant geography and climate-  
286 carbon cycle feedbacks using five Dynamic Global Vegetation Models (DGVMs). *Global*  
287 *Change Biology* **14**, 2015-2039 (2008).
- 288 83. Z. Zhu *et al.*, Greening of the Earth and its drivers. *Nature Climate Change* **6**, 791-795 (2016).
- 289 84. K. C. Samir, W. Lutz, The human core of the shared socioeconomic pathways: Population  
290 scenarios by age, sex and level of education for all countries to 2100. *Global Environmental*  
291 *Change* **42**, 181-192 (2017).
- 292 85. N. Andela *et al.*, A human-driven decline in global burned area. *Science* **356**, 1356-1362  
293 (2017).
- 294 86. F. Li, D. M. Lawrence, B. Bond-Lamberty, Human impacts on 20th century fire dynamics and  
295 implications for global carbon and water trajectories. *Global and Planetary Change* **162**, 18-  
296 27 (2018).

- 297 87. W. Knorr, A. Arneth, L. Jiang, Demographic controls of future global fire risk. *Nature Climate*  
298 *Change* **6**, 781-785 (2016).
- 299 88. F. Li, D. M. Lawrence, B. Bond-Lamberty, Impact of fire on global land surface air temperature  
300 and energy budget for the 20th century due to changes within ecosystems. *Environmental*  
301 *Research Letters* **12**, 044014 (2017).
- 302 89. G. Danabasoglu, NCAR CESM2 model output prepared for CMIP6 CMIP historical. Earth  
303 System Grid Federation. <https://doi.org/10.22033/ESGF/CMIP6.7627>.
- 304 90. J. P. Krasting *et al.*, NOAA-GFDL GFDL-ESM4 model output prepared for CMIP6 CMIP. Earth  
305 System Grid Federation. <https://doi.org/10.22033/ESGF/CMIP6.1407>.
- 306 91. R. Seferian, CNRM-CERFACS CNRM-ESM2-1 model output prepared for CMIP6 CMIP. Earth  
307 System Grid Federation. <https://doi.org/10.22033/ESGF/CMIP6.1391>.
- 308 92. L. M. Ulrike Groemping, Relative Importance of Regressors in Linear Models. [https://cran.r-](https://cran.r-project.org/web/packages/relaimpo/relaimpo.pdf)  
309 [project.org/web/packages/relaimpo/relaimpo.pdf](https://cran.r-project.org/web/packages/relaimpo/relaimpo.pdf) (2021).
- 310 93. M. Z. Al-Hamdan *et al.*, Methods for characterizing fine particulate matter using ground  
311 observations and remotely sensed data: potential use for environmental public health  
312 surveillance. *J Air Waste Manag Assoc* **59**, 865-881 (2009).
- 313 94. H. Hersbach *et al.*, The ERA5 global reanalysis. *Quarterly Journal of the Royal Meteorological*  
314 *Society* **146**, 1999-2049 (2020).
- 315 95. J. X. Wang, J. K. Angell, Air stagnation climatology for the United States. *NOAA/Air Resource*  
316 *Laboratory ATLAS* **1**, <https://www.ncdc.noaa.gov/societal-impacts/air-stagnation/maps>  
317 (1999).
- 318 96. S. Malyshev, E. Shevliakova, R. J. Stouffer, S. W. Pacala, Contrasting Local versus Regional  
319 Effects of Land-Use-Change-Induced Heterogeneity on Historical Climate: Analysis with the  
320 GFDL Earth System Model. *Journal of Climate* **28**, 5448-5469 (2015).
- 321 97. E. Shevliakova *et al.*, Carbon cycling under 300 years of land use change: Importance of the  
322 secondary vegetation sink. *Global Biogeochemical Cycles* **23** (2009).
- 323 98. E. S. Weng *et al.*, Scaling from individual trees to forests in an Earth system modeling  
324 framework using a mathematically tractable model of height-structured competition.  
325 *Biogeosciences* **12**, 2655-2694 (2015).



- 326 99. K. Thonicke, S. Venevsky, S. Sitch, W. Cramer, The role of fire disturbance for global  
327 vegetation dynamics: coupling fire into a Dynamic Global Vegetation Model. *Global Ecology*  
328 *and Biogeography* **10**, 661-677 (2001).
- 329 100. G. P. Compo *et al.*, The Twentieth Century Reanalysis Project. *Quarterly Journal of the Royal*  
330 *Meteorological Society* **137**, 1-28 (2011).
- 331 101. D. M. Lawrence *et al.*, The Land Use Model Intercomparison Project (LUMIP) contribution to  
332 CMIP6: rationale and experimental design. *Geoscientific Model Development* **9**, 2973-2998  
333 (2016).
- 334 102. V. Eyring *et al.*, Overview of the Coupled Model Intercomparison Project Phase 6 (CMIP6)  
335 experimental design and organization. *Geoscientific Model Development* **9**, 1937-1958  
336 (2016).
- 337 103. T. Hajima *et al.*, Development of the MIROC-ES2L Earth system model and the evaluation of  
338 biogeochemical processes and feedbacks. *Geoscientific Model Development* **13**, 2197-2244  
339 (2020).
- 340 104. L. W. Horowitz *et al.*, The GFDL Global Atmospheric Chemistry-Climate Model AM4.1: Model  
341 Description and Simulation Characteristics. *Journal of Advances in Modeling Earth Systems*  
342 **12**, e2019MS002032 (2020).
- 343 105. Ø. Seland *et al.*, Overview of the Norwegian Earth System Model (NorESM2) and key climate  
344 response of CMIP6 DECK, historical, and scenario simulations. *Geosci. Model Dev.* **13**, 6165-  
345 6200 (2020).
- 346 106. S. G. Coles, An Introduction to Statistical Modeling of Extreme Values. *Springer, New York*  
347 (2001).
- 348 107. H. E. Rieder, A. M. Fiore, L. W. Horowitz, V. Naik, Projecting policy-relevant metrics for high  
349 summertime ozone pollution events over the eastern United States due to climate and  
350 emission changes during the 21st century. *Journal of Geophysical Research: Atmospheres*  
351 **120**, 784-800 (2015).
- 352 108. H. E. Rieder, A. M. Fiore, L. M. Polvani, J. F. Lamarque, Y. Fang, Changes in the frequency and  
353 return level of high ozone pollution events over the eastern United States following emission  
354 controls. *Environmental Research Letters* **8**, 014012 (2013).

- 355 109. L. Shen, L. J. Mickley, E. Gilleland, Impact of increasing heat waves on U.S. ozone episodes in  
356 the 2050s: Results from a multimodel analysis using extreme value theory. *Geophys Res Lett*  
357 **43**, 4017-4025 (2016).
- 358 110. E. Gilleland, R. W. Katz, extRemes2.0: An Extreme Value Analysis Package in R. *Journal of*  
359 *Statistical Software* **72** (2016).
- 360 111. D. Bolton, The Computation of Equivalent Potential Temperature. *Monthly Weather Review*  
361 **108**, 1046-1053 (1980).
- 362 112. J. X. L. Wang, J. K. Angell, Air stagnation climatology for the United States (1948--1998).  
363 *NOAA/Air Resources Laboratory ATLAS No.1* (1999).
- 364 113. D. E. Horton, C. B. Skinner, D. Singh, N. S. Diffenbaugh, Occurrence and persistence of future  
365 atmospheric stagnation events. *Nature Climate Change* **4**, 698-703 (2014).
- 366 114. J. W. Hurrell *et al.*, The Community Earth System Model: A Framework for Collaborative  
367 Research. *Bulletin of the American Meteorological Society* **94**, 1339-1360 (2013).
- 368
- 369